Journal of Contaminant Hydrology 233 (2020) 103656

Contents lists available at ScienceDirect

Journal of Contaminant Hydrology

journal homepage: www.elsevier.com/locate/jconhyd

Whale burial and organic matter impacts on biogeochemical cycling in beach aquifers and leachate fluxes to the nearshore zone

James W. Heiss*,[1]

Department of Environmental, Earth and Atmospheric Sciences, University of Massachusetts Lowell, USA

ARTICLE INFO

Keywords:
Beach aquifer
Biogeochemical processes
Groundwater-surface water interactions
Submarine groundwater discharge
Whale burial

ABSTRACT

Coastal managers are increasingly faced with the challenge of disposing of stranded whale carcasses on beaches. Direct burial in the beach is often used as a cost effective method of disposal. However, whale burial management plans are often met with public resistance owing to the perceived risk of shark attraction to burial leachate that may discharge from the seabed. A reactive transport model was combined with a numerical variable-density groundwater flow model to assess buried whale leachate plume formation, transport, influence on beach aquifer reactivity, and discharge to coastal surface water for a range of burial setback distances, depths, and whale sizes. A second set of simulations was performed to evaluate aquifer nitrate removal efficiencies for a range of buried wrack scenarios and to evaluate the role of organic carbon source on beach reactivity. A sensitivity analysis was performed for both sets of models across ten physical and reaction parameters. Simulations using the best estimate parameter set showed that whale burials can produce DOC and ammonium leachate plumes in the beach aquifer that are transported to and discharge near the low tide line in water depths of 0.4–2.4 m. DOC and ammonium concentrations in discharging whale leachate were1.6 and 26 times higher than typical surf zone concentrations, respectively. Of the factors tested, the burial distance inland from the high tide line was the most important factor affecting leachate fluxes to surface water. Burials placed farther inland led to smaller DOC fluxes to surface water, but increased ammonium fluxes. Burial depth also affected whale leachate to the subtidal zone, with deeper burials resulting in smaller fluxes of DOC. Leached DOC from whale decomposition and from buried wrack can fuel denitrification hotspots within beach sediments. The sensitivity analysis showed that nitrate removal supported by buried wrack and whale leachate fluxes are highly dependent on beach properties, hydrologic forcing, and reaction parameters. The wrack model results have implications for beach scraping and the whale burial models show that whale leachate can be delivered to the shallow subtidal zone via groundwater discharge pathways, with potential implications for shark attraction and whale burial management practices.

1. Introduction

The discharge of fresh groundwater across the seabed (submarine groundwater discharge; SGD) is a primary vector of nutrient, heavy metal, and contaminant delivery to the surf zone and coastal ocean ecosystems. These SGD-borne solutes can contribute to the formation and maintenance of algal blooms (Lecher et al., 2015; Paerl, 1997), affect fish production (Fujita et al., 2019), decrease coral cover and species diversity (Amato et al., 2016; Crook et al., 2012; Lirman et al., 2003), result in loss of seagrass habitat (Valiela et al., 1997), and have cascading effects across trophic levels (Lecher and Mackey, 2018). The impacts of groundwater chemical fluxes to the surf zone are compounded by the large volume of fresh SGD, which is estimated to be 6–10% of global river runoff (Zektser and Loaiciga, 1993), and higher in other coastal watersheds (Russoniello et al., 2016). Prior to discharge, nutrient-rich groundwater can undergo biogeochemical processing in beach aquifers that transforms nutrients to non-bioavailable solutes. The formation of the reactive zones along groundwater discharge pathways depends on the availability of reactants supplied by the physical groundwater flow system (Anwar et al., 2014; Heiss et al., 2017; Spiteri et al., 2008b). Thus, it is important to characterize and quantify chemical delivery to the coastal zone via SGD in the context of the interplay between physical and biogeochemical processes in coastal aquifers.

* Corresponding author.
E-mail address: James_Heiss@uml.edu.
[1] One University Ave., University of Massachusetts Lowell, Lowell, MA, 01854.

https://doi.org/10.1016/j.jconhyd.2020.103656
Received 25 October 2019; Received in revised form 14 April 2020
Available online 27 May 2020

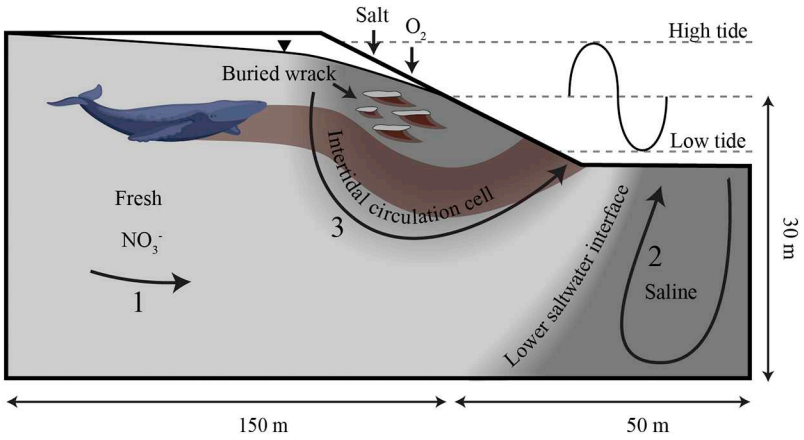

Fig. 1. Conceptual model of whale burial and organic carbon aggregate (wrack) leachate and discharge to surface water along groundwater flow pathways in a beach aquifer under tidal influence. Process 1 is terrestrially-driven fresh groundwater flow. Process 2 is density-driven saltwater circulation, and Process 3 is tidally-driven intertidal circulation and mixing.

Large marine vertebrates such as whales are often strand on beaches. The number of whale carcass strandings have risen with whale populations since the 1986 commercial whaling moratorium (Tulloch et al., 2018). Along the east coast of South America, for example, there were a total of 11,761 documented strandings between 1976 and 2013 (Prado et al., 2016). Whale strandings in densely populated areas can detract beachgoers due to odors and unattractive sight during decomposition, potentially impacting local tourist economies. To combat these issues, beach managers implement several disposal methods to remove whale carcasses from the beach, including offshore towing, transport to a waste facility, and beach burial.

Beach burial is the primary means of whale and other cetacean carcass disposal and is common in densely populated areas where recreational activity would be adversely impacted if the stranding were not removed. The possible impacts of beach burial include 1) biogeochemical alteration of beach groundwater and 2) shark attraction to the burial vicinity from leaching of DOC and nutrients into surrounding groundwater and subsequent discharge to surface water (Tucker et al., 2018). The concern of shark attraction likely stems from the known behavior of sharks, such as White (Fallows et al., 2013) and Tiger Sharks (Clua et al., 2013), that feed on floating whale carcasses (Tucker et al., 2019). While potential whale burial impacts are unclear, there remains a strong public resistance to burials due to the perceived risks.

Despite the potential impacts, the effects of beach whale burials on nutrient cycling and chemical fluxes to the surf zone are unclear owing to the limited number of existing studies. Tucker et al. (2019) conducted a laboratory study of the effects of whale burials on beach pore water chemistry and showed through column experiments that whale decomposition following burial resulted in a DOC, NH_4^+, and PO_4^{3-} leachate plume that extended up to 2.5 m from the burial location. A field burial in the unsaturated zone of a beach in the same study provided no clear temporal or spatial trends in NO_3^-, or PO_4^{3-} concentrations in the beach subsurface. Tucker et al. (2019) concluded that whale burial leachate plumes would unlikely serve as a shark attractant due to the short leachate travel distance through the beach subsurface. To the author's knowledge, Tucker et al. (2019) is the only study to investigate whale burial impacts on beach pore water chemistry. Decomposition leachate is likely to develop down-gradient from a whale burial and may be transported to the subtidal zone due to 1) shallow beach water tables that inundate burials, 2) seawater infiltration across the beachface that transports oxygen into the aquifer to support decomposition, and 3) rapid circulating flow paths leading from typical burial locations to regions of groundwater discharge in the surf zone (Robinson et al., 2007b; Xin et al., 2010). A more complete understanding of the interactions between whale burials and groundwater dynamics in beach aquifers is needed to inform management decisions to minimize potential adverse impacts of burials on surface water quality and to provide insight into the potential risk of shark attraction to recreational beaches.

In addition to megafauna, wave and tidal action on sandy beaches deposit algae, intertidal invertebrates, small crustaceans, woody debris, and drift macrophytes, the latter originating from offshore reefs, kelp forests, and seagrass beds. This organic matter, collectively termed beach wrack, is deposited across the upper, middle, and lower intertidal zone (Orr et al., 2005). Tidally deposited algal and macrophyte wrack can provide large quantities of organic material to the supratidal interface, with deposits of up to 3.5 kg per meter length of shoreline per tidal cycle (Orr et al., 2005). The organic matter undergoes degradation and burial as the beach profile cycles through accretionary and depositional stages (Dugan et al., 2011; Ford et al., 1999). Combined with permeable intertidal sediments, spatially heterogeneous buried wrack may provide a significant organic carbon source to the beach aquifer microbial community (Rossi and Underwood, 2002). For instance, aggregates of particulate organic carbon (POC) can lead to the development of denitrification microzones in aquatic (Sawyer, 2015) and marine (Sakita and Kusuda, 2000) sediments, and can leach DOC that fuels aerobic respiration and denitrification in beach aquifers (Kim et al., 2019).

Groundwater flow patterns and the distribution of fresh and saline groundwater in coastal aquifers is controlled by interactions between coastal ocean and terrestrial hydrologic forcings (Fig. 1). Fresh groundwater from terrestrial recharge flows seaward where it mixes with saltwater to form a lower saltwater (Ghyben-Herzberg) interface. Density gradients between fresh and saline groundwater along the lower saltwater interface drive convective flow where seawater infiltrates into the seabed offshore which then circulates upward along the interface (process 2; Fig. 1) (Cooper, 1959; Kohout, 1960). Tidal and wave activity on the sloping beach results in infiltration of seawater and a hydraulic gradient that drives flow downward and seaward, forming an intertidal circulation cell (process 3; Fig. 1) that is bounded by a saltwater-freshwater mixing zone (Abarca et al., 2013; Boufadel, 2000; Heiss and Michael, 2014; Michael et al., 2005; Robinson et al., 2006; Turner and Acworth, 2004; Ullman et al., 2003; Vandenbohede and Lebbe, 2005; Xin et al., 2010). A fresh groundwater discharge zone located near the base of the beach separates the intertidal circulation cell from the lower saltwater interface.

A wide range of microbially mediated redox reactions have been observed in beach aquifers, including aerobic respiration (Slomp and Van Cappellen, 2004), denitrification (Santos et al., 2009), iron reduction (Roy et al., 2010), sulfate reduction (McAllister et al., 2015), and dissimilatory nitrate reduction to ammonium (Santoro, 2010). These biogeochemical processes influence the cycling of C, N, P, Fe, and other metals, altering the chemistry of groundwater discharging to coastal surface water. Field studies demonstrate that flowpaths and residence times are important factors influencing the location and type of redox activity within the intertidal mixing zone (Charette and

Sholkovitz, 2006; McAllister et al., 2015; Slomp and Van Cappellen, 2004), while numerical models have been used to isolate the key physical (e.g. hydraulic conductivity, beach slope) and hydrologic (tidal amplitude, freshwater flux) controls on biogeochemical processing in beach sediments (Anwar et al., 2014; Heiss et al., 2017; Robinson et al., 2009; Spiteri et al., 2008b). Most conceptual and numerical models assume that infiltrating seawater across the beach surface is the source of DOC that fuels beach reactivity.

Field observations reveal that the distribution of organic carbon and reactivity in the intertidal mixing zone can be spatially heterogeneous despite homogeneous aquifer material (Kim et al., 2017; Seibert et al., 2019). The reactive hotspots within the beach aquifer can be fueled by scattered carbon pools that form as a result of filtering of circulating DOC-rich seawater and the differential accumulation of DOC on intertidal sediments (Kim et al., 2019). In addition, in-situ organic-rich aggregates may derive from the deposition and burial of organic debris (i.e. wrack) deposited in the intertidal zone owing to wave and tidal action, promoting the formation of reactive hotspots in the aquifer (Seidel et al., 2015). Sediment carbon pools are important for aquifer reactivity in other environments as well. For example, spatially heterogeneous carbon aggregates can drive localized denitrification in streambed sediments and significantly alter nitrate fluxes to aquatic ecosystems (Sawyer, 2015). Laboratory experiments have also shown that whale burials can serve as a source of carbon for beach microbial communities (Tucker et al., 2019).

In this study, I apply numerical groundwater flow and reactive transport models to evaluate nutrient cycling in coastal aquifers for a range of whale burial and buried wrack scenarios for beaches exposed to tides. A sensitivity analysis of whale size, burial depth, and distance inland from the high tide line is performed for a range of values obtained from whale burial reports to identify the key factors controlling beach aquifer reactivity and to assess whale leachate fluxes to the subtidal zone. Simulations involving buried wrack aggregates are performed to provide additional insight into the role of in-situ particulate organic carbon (POC) on beach aquifer reactivity.

2. Methods

Groundwater flow and reactive transport models were used to simulate the effects of whale burials on chemical transport in beach aquifers for a range of burial distances inland from the high tide line (hereafter referred to as *setback distance*), burial depth, and whale size. Whale burial setback distance, burial depth, and whale size were determined by compiling whale burial media reports (Table 1). Whale burials have rarely been the focus of scientific investigations (Bui, 2009; Tucker et al., 2019) and thus formal reporting is scarce. In the models, the setback distance ranged from 0 to 30 m, burial depth from 2 to 8 m, and whale length from 9 to 15 m. Whale width (height) was estimated using the length-to-width ratio (3.9) of adult female Right Whales (Miller et al., 2012). The whale burials in the models were represented as permeable carbon-rich sediment, hereafter referred to as POC. The organic carbon content of the sediment is discussed later in this section. Setback distance, burial depth, and whale size was varied around a *base case parameter set* adopted from Spiteri et al., 2008a and other studies with calibrated models or measurements (Table 2). A subset of the parameter set was previously calibrated to measurements from a beach aquifer (Spiteri et al., 2008b). A sensitivity analysis was performed around the base case parameter set for a *base case whale burial scenario* (10 m setback distance, 4 m burial depth, 12 m length) to evaluate the effects of 10 model parameters on DOC and ammonium leachate fluxes across the sediment-water interface (Table 3). Literature values were used to bound the range of each parameter.

A second set of simulations was performed to assess the effects of buried wrack aggregates on chemical cycling in the aquifer. To incorporate realistic distributions of buried wrack, Gaussian random-fields were generated geostatistically using the sequential Gaussian

Table 1
Whale burial examples as described by media outlets that reported either burial depth, burial location, or both. n/a = not available.

Location	Year	Whale length [m]	Species	Burial depth [m]	Setback distance [m]	Reference
Sharp Park Beach, CA, USA	2015	12.8	Humpback	5	15	https://www.sfgate.com/bayarea/article/Burial-at-the-beach-Rotting-whales-going-more-6273109.php
Duxbury, MA, USA	2018	15.8	Fin	6	n/a	https://www.bostonglobe.com/metro/2018/08/21/cause-death-sought-dead-fin-whale-buried-duxbury/WcF926Ta56mdpcsqvNhnZN/story.html
Raigad, India	2015	13.7	Blue	n/a	High tide line	https://www.dnaindia.com/india/report-beached-blue-whale-cremated-after-initial-burial-fails-2100077
Nobbys Beach, NSW, Australia	2017	12	n/a	4	10	https://www.abc.net.au/triplej/programs/hack/how-do-you-dispose-of-a-dead-whale/8968882
Ocean Grove, VIC, Australia	2018	n/a	n/a	2.5	Behind dune	https://www.abc.net.au/news/2018-11-22/coastal-community-anger-over-department-decision-to-bury-whale/10518358
Grassy Head beach, NSW, Australia	2016	14	Humpback	n/a	Behind dune	https://www.nambuccaguardian.com.au/story/4144738/washed-up-whale/
Breezy Point, NY, USA	2012	18.2	Fin	n/a	Behind dune	https://www.cnn.com/2012/12/27/us/ny-beached-whale/index.html
San Francisco, CA, USA	2010	15.4	Fin	n/a	Backshore	https://sanfrancisco.cbslocal.com/2010/09/21/whale-being-buried-at-ocean-beach-after-washing-ashore/
Agate Beach, OR, USA	2017	12.2	Gray	n/a	Backshore	https://www.newslincolncounty.com/archives/182893
Port Aransas, TX, USA	2010	14.6	n/a	4	In front of dune	https://www.portasouthjetty.com/articles/whale-of-a-burial/
Huntington Beach, CA, USA	2019	7.6	n/a	5	Backshore	https://www.ocregister.com/2019/06/04/dead-whale-is-buried-in-sand-at-huntington-beach-after-several-attempts-to-tow-it-back-to-the-ocean/
Broadwater Beach, NSW, Australia	2016	n/a	n/a	n/a	Behind dune	https://www.northernstar.com.au/news/whale-buried-amongst-the-sand-dunes/3113329/#/0
Wurtulla Beach, QLD, Australia	2017	9	n/a	3	30	https://www.sunshinecoastdaily.com.au/news/fate-of-wurtulla-beach-whale-carcass-decided/3240869/
Pacifica, CA, USA	2015	14.6	Sperm	n/a	Backshore	https://patch.com/california/sanbruno/two-beached-whales-be-buried-beach
South Ballina, NSW, Australia	2017	n/a	Humpback	n/a	150	https://www.abc.net.au/news/2017-10-11/whale-carcass-disposals-on-nsw-north-coast-beaches-reckless/9038046
Kings Beach, CA, USA	2009	14	Sperm	3	Backshore	https://www.brisbanetimes.com.au/national/queensland/rotting-whale-carcass-buried-at-sunshine-coast-beach-20090519-bdw4.html

Table 2
Reaction parameter values for the base case heterogeneous POC and whale burial model base cases.

Parameter	Unit	Description	Base case [Whale Burial]	Base case [Wrack]
k_{fox}	s^{-1}	Rate constant for decomposition of DOC	6×10^{-9}[c]	5×10^{-7}[a]
kmo2	M	Limiting concentration of O_2	3.125×10^{-5}[ab]	3.125×10^{-5}[a, b]
kmno3	M	Limiting concentration of NO_3^-	8.065×10^{-6}[ab]	8.065×10^{-6}[a,b]
k_{nit}	$M^{-1}\ s^{-1}$	Rate constant for nitrification	0.159[e]	0.159[e]
β_{O_2}	–	Stoichiometric coefficient for aerobic respiration	1	1
β_{NO_3}	–	Stoichiometric coefficient for denitrification	0.8	0.8
τ_{NC}	–	Ratio of NH_4^+ produced to C mineralized	0.104	0.104
α	s^{-1}	Mass transfer coefficient for organic carbon	2.78×10^{-8}[d]	2.78×10^{-8}[d]
K_d	$m^3\ kg^{-1}$	Distribution coefficient for organic carbon	94[c]	10[d]
α_L	m	Longitudinal dispersivity	0.5[f]	0.5[f]
α_T	m	Transverse dispersivity	0.05[f]	0.05[f]
θ	–	Porosity	0.3	0.3

[a] Van Cappellen and Wang (1996)
[b] Bardini et al. (2012).
[c] Tucker et al. (2019).
[d] Zarnetske et al. (2012).
[e] Billen et al. (1982).
[f] Heiss and Michael (2014).

simulation algorithm in SGeMS (Remy et al., 2009). The Gaussian-random fields were then truncated using arbitrary threshold values corresponding to proportions of wrack in the intertidal sediment. The buried wrack, or POC aggregates, represented macrophytes, sticks, invertebrates, and other organic matter debris. The overall spatial extent of the POC aggregates was assigned according to the area in the circulation cell where pore water was >1 ppt to ensure that POC was located between the high and low tide levels where wrack is deposited. Nine wrack deposit realizations were generated with POC-rich sediments comprising 10–90% of intertidal circulation cell sediments. The whale burial and buried wrack scenarios were modeled separately in order to isolate the individual effects of the two organic carbon sources on nitrogen cycling in the coastal aquifer. The same physical and geochemical parameter set used in the whale burial models was used in the wrack models. A wrack sensitivity analysis was performed across the same 10 physical and geochemical parameters that were tested in the whale burial sensitivity (Table 3). This second sensitivity analysis was used to assess the spectrum of nitrate removal efficiencies that may be expected across physical and geochemical parameter space for intertidal POC contents ranging from 10 to 100%. A total of 467 simulations were performed.

In addition to buried organic matter, tides can introduce DOC-rich seawater to sediments through infiltration across the shoreface, which can serve as a source of carbon to drive microbial activity in intertidal mixing zones (Anwar et al., 2014; Kim et al., 2019; Seidel et al., 2015). An additional simulation was performed with infiltrating seawater as a source of DOC to compare to the whale burial and wrack aggregate scenarios to assess the relative importance of DOC source on microbially mediated chemical transformations. This simulation is hereafter referred to as the *baseline simulation*. POC served as the only source of DOC in the whale burial and wrack deposit scenarios.

Density-dependent groundwater flow and salt transport was simulated using SEAWAT v4.0 (Langevin et al., 2008). The model domain and boundary conditions were similar to previous modeling studies of groundwater flow in beach aquifers (e.g. Greskowiak, 2014; Heiss and Michael, 2014; Robinson et al., 2006; Robinson et al., 2007a, 2007b, 2007c). The model domain extended 150 m landward of the shoreline, 50 m seaward of the shoreline, and to a depth of 30 m below MSL. The beach slope was 0.1 in the base case models. The grid was non-uniform and refined in the intertidal zone ($\Delta x = 0.31$ m, $\Delta y = 0.06$ m). The third-order total-variation-diminishing (TVD) scheme was used to solve the advection term. The Periodic Boundary Condition package (Post, 2011) was used to simulate tidal forcing and seepage face development across the aquifer-ocean interface. A time-dependent hydraulic head signal was applied to the intertidal and subtidal zone, with the hydraulic head h_t at the boundary defined as

$$h_t = A\cos(\omega t) + h_o \quad (1)$$

where h_t (m) is the tidal elevation at time t, A (m) is the tidal amplitude, ω ($= \frac{2\pi}{T}$) is the tidal angular frequency in rad d^{-1}, and h_o (m) is a reference water level (MSL). In all models, $A = 1.0$ m and $\omega = 12.567$ rad d^{-1}. Model cells along the shoreface with inflow were

Table 3
Model parameters and literature sources used in the sensitivity analysis. Parameters for the whale burial and wrack simulations are the same unless noted.

Parameter	Unit	Description	Base case	Sensitivity range	Source
A	m	Tidal amplitude	1.0	0.25–1.35	3
K_x	m/d	Horizontal hydraulic conductivity	8.6	2–50	1, 4, 12
K_y/K_z	m/d	Hydraulic conductivity anisotropy ratio	1.0	0.1–1.0	1, 4, 12
β	–	Beach slope	0.1	0.375–0.1	1
α_L	m	Longitudinal dispersivity	0.5	0.1–1.0	5
α_T/α_L	m	Transverse dispersivity ratio	0.1	0.01–0.2	5
i	–	Freshwater hydraulic gradient	6.7×10^{-3}	3×10^{-3} - 8.3×10^{-3}	2
k_{fox}	s^{-1}	Rate constant for decomposition of DOC	6×10^{-9} (whale) 5×10^{-7} (wrack)	6×10^{-9} - 1.5×10^{-7}	6, 11
α	s^{-1}	Mass transfer coefficient for organic carbon	2.78×10^{-8}	2.78×10^{-9} - 2.78×10^{-7}	7, 8, 9
K_d	$m^3\ kg^{-1}$	Distribution coefficient for organic carbon	94 (whale) 5 (wrack)	5–100	8, 9, 10

Literature sources: 1) Hazen (1911), 2) Heiss et al. (2017), 3) Hill (2016), 4) Reis and Gama (2010), 5) Gelhar et al. (1992), 6) Van Cappellen and Wang (1996), 7) Jardine et al. (1992), 8) MacQuarrie et al. (2001), 9) Gu et al. (2007), 10) Robertson and Cherry (1995), 11) Tucker et al., 2019, 12) Todd (1980).

assigned a zero-concentration gradient and cells with discharge were assigned a constant concentration of 35 ppt. The hydraulic head at the landward vertical boundary was set to 1.0 m and the top, bottom, and right boundaries were assigned as no flow and zero solute flux.

The phase-resolved flow fields from the SEAWAT simulations were used with the multi-species reactive transport model PHT3D v2.13 (Prommer and Post, 2003) to simulate aerobic respiration, denitrification, nitrification, ammonification, and POC dissolution. The reaction time steps in PHT3D were set to correspond with the transport steps in SEAWAT used to satisfy numerical stability criteria. The reaction network and rate expressions for aerobic respiration, denitrification, and nitrification were adopted from previous modeling studies of geochemical reactions in coastal groundwater systems (Anwar et al., 2014; Cardenas et al., 2008; Spiteri et al., 2008b):

Aerobic respiration (AR)

$$(CH_2O)_y(NH_3)_z + yO_2 \rightarrow zNH_4^+ + yCO_2 + yH_2O \quad (2)$$

Denitrification (DN).

$$(CH_2O)_y(NH_3)_z + 0.8yNO_3^- \rightarrow zNH_4^+ + 0.4N_2 + (0.2y-z)CO_2 + (0.8y + z)HCO_3 + (0.6y-z)H_2O \quad (3)$$

Nitrification (NI)

$$NH_4^+ + 2O_2 + 2HCO_3^- \rightarrow NO_3^- + CO_2 + 3H_2O \quad (4)$$

Ammonification (AM)

$$\{NH_3\}_{POC} \rightarrow NH_4^+ \quad (5)$$

where y and z represent the C:N ratio of 106:11 in coastal environments (Van Cappellen and Wang, 1996). The rate expressions for the reactions are the following:

$$R_{AR}\begin{cases} If\ [O_2] > kmo2;\ k_{fox}[DOC] \\ If\ [O_2] < kmo2;\ k_{fox}[DOC]\left(\frac{[O_2]}{kmo2}\right) \end{cases} \quad (6)$$

$$R_{DN} = \begin{cases} If\ [O_2] > kmo2;\ 0 \\ If\ [O_2] < kmo2\ and\ [NO_3^-] > kmno3;\ k_{fox}[DOC]\left(1 - \frac{[O_2]}{kmo2}\right) \\ If\ [O_2] < kmo2\ and\ [NO_3^-] < kmno3;\ k_{fox}[DOC]\left(1 - \frac{[O_2]}{kmo2}\right)\left(\frac{[NO_3^-]}{kmno3}\right) \end{cases} \quad (7)$$

$$R_{NI} = k_{nit}[O_2][NH_4^+] \quad (8)$$

where $kmo2$ is the limiting O_2 concentration, k_{fox} is the DOC rate constant, $kmno3$ is the limiting NO_3^- concentration, and k_{nit} is the rate constant for nitrification. The reduction rate of O_2 and NO_3^- proceeds according to a linearized Monod formulation whereby the availability of the electron acceptor inhibits the reduction rate when the concentration falls below the limiting O_2 or NO_3^- concentration (Bardini et al. 2012; Spiteri et al., 2008b). When the concentration is above the limiting concentration, the reduction rate of O_2 and NO_3^- follows a first-order reaction and the rate is independent of the concentration. The stoichiometry of aerobic respiration and denitrification is accounted for using the stoichiometric coefficients for each reaction (Table 2).

The terminal N product of DOC mineralization is represented as NH_4^- and is produced via ammonification, assuming the C:N stoichiometry of coastal environments ($\tau_{NC} = 1/9.6$) in the ratio of NH_4^- produced to C mineralized (Van Cappellen and Wang, 1996):

$$R_{AM} = \tau_{NC} k_{fox}[\mathrm{DOC}] \quad (9)$$

DOC production is coupled to the decomposition of POC using a linear first-order kinetic dissolution model (Jardine et al., 1992; Sawyer, 2015; Zarnetske et al., 2012):

$$R_{\mathrm{DOC\_PROD}} = \alpha(K_d[\mathrm{DOC}] - [\mathrm{POC}]) \quad (10)$$

where R_{DOC_PROD} is the DOC production rate due to POC decomposition, α is the first-order mass transfer coefficient between POC and DOC, and K_d is the distribution coefficient. DOC degradation was assumed a linear-first order reaction (Anwar et al., 2014; Bardini et al., 2012; Spiteri et al., 2008):

$$R_{DOC\_DECAY} = k_{fox}[DOC] \quad (11)$$

Thus, the net change in DOC is the DOC generated in Eq. 10 less the DOC degradation in Eq. 11. The redox reactions are coupled to the degradation of DOC using the partial equilibrium approach that assumes: 1) the oxidation of DOC is the rate limiting step in the reactions and 2) the reduction step is instantaneous (Brun and Engesgaard, 2002; Postma and Jakobsen, 1996; Quanrud et al., 1996; Spiteri et al., 2008a). Model parameters in the flow and reactive transport simulations are within the range of published values (Table 2). The DOC rate constant in the whale burial models was obtained from laboratory experiments of whale carcass decomposition in beaches (Tucker et al., 2019).

The landward vertical boundary was assigned a constant NO_3^- concentration to represent inflowing NO_3^--rich fresh groundwater. Seawater entering the aquifer at the shoreface boundary contained salt and O_2, and for the case with seawater as the source of organic carbon, DOC. Oxygen replenishment to pore water from the atmosphere (e.g. Geng et al., 2015) was not incorporated into the model. Specified concentrations of DOC (2×10^{-3} M), O_2 (3.13×10^{-4} M), NO_3^- (1.29×10^{-4} M) were characteristic of concentrations in coastal sediments (Berner, 1981; Van Cappellen and Wang, 1996).

POC concentrations were assigned for each of the two sets of whale burial and wrack deposit models. The POC concentration for the whale burials was set to 1.27 M (~1% organic carbon content) following previous laboratory experimental setups of whale carcass leachate in beach aquifers (Tucker et al., 2019). The POC concentration of wrack aggregates was 8.33×10^{-3} M (0.1% organic carbon content), which was assigned using measured POC pore water concentrations in beach sands (Kim et al., 2017) and the distribution coefficient (Table 2). The organic carbon content of the wrack aggregates is within the range of organic carbon content of intertidal beach sands (Huettel and Rusch, 2000).

3. Results

3.1. Baseline solute concentrations and reactivity

Tidal oscillations and seawater infiltration across the shoreface in the baseline simulation produced circulating flows in the beach aquifer, where seawater flowed downward and to the base of the beach while mixing with underlying fresh groundwater to form a saltwater-freshwater mixing zone (Fig. 2a). The simulated flow pattern and mixing zone is consistent with previous modeling studies of beach groundwater dynamics (Boufadel, 2000; Heiss and Michael, 2014; Lebbe, 1999; Robinson et al., 2006). DOC concentrations were elevated in the shallow beach subsurface where seawater infiltration was highest and decreased with depth due to DOC degradation (Fig. 2b). Mineralization of DOC maintained elevated NH_4^+ concentrations in the circulation cell (Fig. 2c). DOC oxidation was coupled to aerobic respiration, so O_2 concentrations were low throughout the intertidal circulation cell (Fig. 2d). However, O_2 concentrations were sufficient to maintain nitrification directly beneath the high tide line to a depth of 2 m (Fig. 2e). Farther landward and at depth, anoxia along the boundary of the circulation cell produced favorable conditions for denitrification, which was highest on the landward side of the circulation cell where DOC and NO_3^- were abundant (Fig. 2f). Denitrification within this region of the aquifer produced N_2 that was transported to the lower part of the beachface (Fig. 2g). Nitrate attenuation as a percent of total inflowing

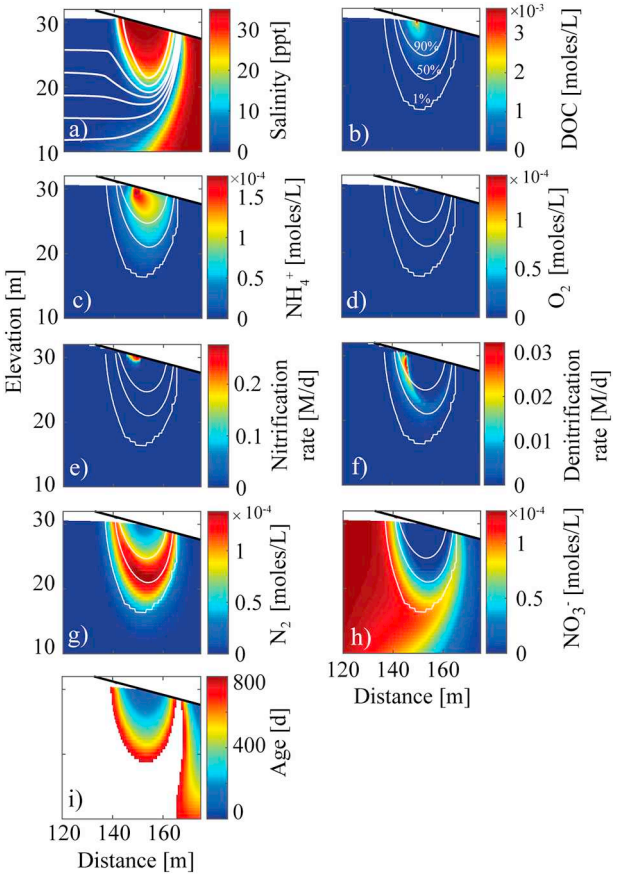

Fig. 2. Model results for the baseline simulation without a whale burial or buried wrack. a) salinity and phase-averaged flow streamlines, b) DOC, c) O_2, d) NO_3^-, e), N_2 f) NH_4^+, g) nitrification rates, h) denitrification rates, i) groundwater age. White contours are 1%, 10% and 90% seawater salinity.

land-derived nitrate, defined as nitrate removal efficiency, was 37.4% for the baseline simulation.

3.2. Whale burials: solute concentrations and reaction zones

The whale burials altered the chemical composition of pore water in the beach aquifer for the base case set of models (Fig. 3). Decomposition of the burials led to localized areas of elevated DOC concentrations, which decreased along flowpaths owing to DOC oxidation (Fig. 3, column 2). DOC concentrations surrounding and down-gradient of burials with a setback distance of 0 m were lower relative to burials at the same depth 20 m inland (Fig. 3, rows a-b). Burial depth also influenced spatial patterns of DOC. DOC concentrations surrounding burials at 2 m depth were lower than burials at 8 m depth for the same setback distance (Fig. 3, rows c-d). The variability in DOC concentrations for different setback distances and burial depths is owed to the burial location relative to the intertidal circulation cell. For a 0 m setback distance, pore water circulating at high velocity below the high tide line readily flushed DOC out of the system, while the burial with a 20 m setback distance was landward of the circulation cell where flow rates were lower, allowing DOC to accumulate. Similarly, burial depth controlled the proximity of the carcass relative to the circulation cell. Deeper burials with the same setback distance were offset horizontally from intertidal flows because the circulation cell tapered with depth. The low flow velocities outside of the circulation cell led to the accumulation of DOC. Lastly, larger whale burials produced more DOC and resulted in higher down-gradient DOC concentrations (Fig. 3, rows e-f).

Burial location was a key factor controlling NH_4^+ distributions and nitrification rates (Figs. 3 and 4). Regions of elevated NH_4^+ concentrations developed due to DOC degradation and ammonification. For a setback distance of 20 m, NH_4^+ accumulated along flow paths leading to the intertidal mixing zone (Fig. 3, row 2). Low NH_4^+ concentrations were maintained within the interior of the circulation cell (>90% seawater) as a result of nitrification and subsequent removal of NH_4^+ in oxygen-rich pore water. Nitrification rates were highest 1–3 m below the high tide line where infiltration of oxygen-rich seawater was highest (Fig. 4). The location of the nitrification zone was unaffected by whale burial distance inland, depth, or whale size because circulating flows in the mixing zone hydraulically restricted the extent of overlap between NH_4^+ and O_2.

Nitrate concentrations varied with typical setback distances, burial depths, and whale sizes. Nitrate-rich fresh groundwater flowing into the aquifer was anoxic and thus burials inland of oxygenated intertidal pore water formed denitrification hotspots (Fig. 3, row 4). Denitrification rates within the hotspots increased with setback distance and reached a maximum of 2.5×10^{-3} M/d (Fig. 5). In the case of a 20 m setback distance, slow transport rates and a high accumulation of DOC in the freshwater aquifer promoted rapid NO_3^- uptake, which formed a large region of low NO_3^- concentrations that merged with the circulation cell (Fig. 3, row b). NO_3^- uptake was limited for burials located in the circulation cell due to the presence of O_2 from infiltrating seawater and lower DOC concentrations from rapid flushing of intertidal pore water (Figs. 5a).

Simulated DOC and ammonium concentrations were elevated relative to observed data reported in literature, while nitrate concentrations compare favorability with measured values in previous studies. The maximum leached DOC concentration (6.1×10^{-3} M) was greater than the range of highest DOC concentrations (2.5×10^{-4} - 3.0×10^{-3} M) observed in natural beach aquifers (e.g. Santos et al., 2008; Seidel et al., 2015; Spiteri et al., 2008a). Modeled ammonium concentrations (maximum 1.8×10^{-4} M) were near the upper end of the range (4.0×10^{-5}–2.4×10^{-4} M) of values measured in beach sediments (Kim et al., 2017; Kroeger and Charette, 2008; Spiteri et al., 2008a; Ullman et al., 2003). Nitrate concentrations in the intertidal mixing zone (1–90% seawater salinity) ranged from 1.3×10^{-4} M – 1.4×10^{-5} M, consistent with observed concentrations reported in literature (e.g. Couturier et al., 2017; Charbonnier et a., 2013; Kroeger and Charette, 2008).

3.3. Whale burials: nitrate removal

The three physical burial factors affected the flux of land-derived NO_3^- across the aquifer-ocean interface. Nitrate removal efficiency increased with setback distance and ranged from 41 to 52%, reaching an asymptote at a setback distance of 20–30 m (Fig. 6a). Removal efficiency increased from 50 to 58% with an increase in burial depth from 2 to 8 m (Fig. 6b). Deeper burials were located farther outside of the circulation cell relative to shallow burials because the cell tapered with depth, as discussed previously. This offset had a similar effect as high setback distances; slower transport rates outside of the circulation cell led to the accumulation of DOC and longer residence times that enhanced reactivity. Removal efficiency increased from 24 to 68% as whale length increased from 9 to 15 m as a result of higher DOC production (Fig. 6c).

3.4. Total whale leachate flux to the subtidal zone

Leachate fluxes to surface water were nonzero for the range of setback distances, burial depths, and whale sizes considered. DOC flux decreased with increasing setback distance because longer flow paths lead to greater DOC degradation (Fig. 6d). An increase in burial depth led to lower DOC fluxes due to greater DOC degradation along slow transport paths adjacent to the circulation cell (Fig. 6e). Whale size was also a key factor controlling leachate flux. Decomposition of larger burials generated larger quantities of DOC, thus DOC fluxes increased

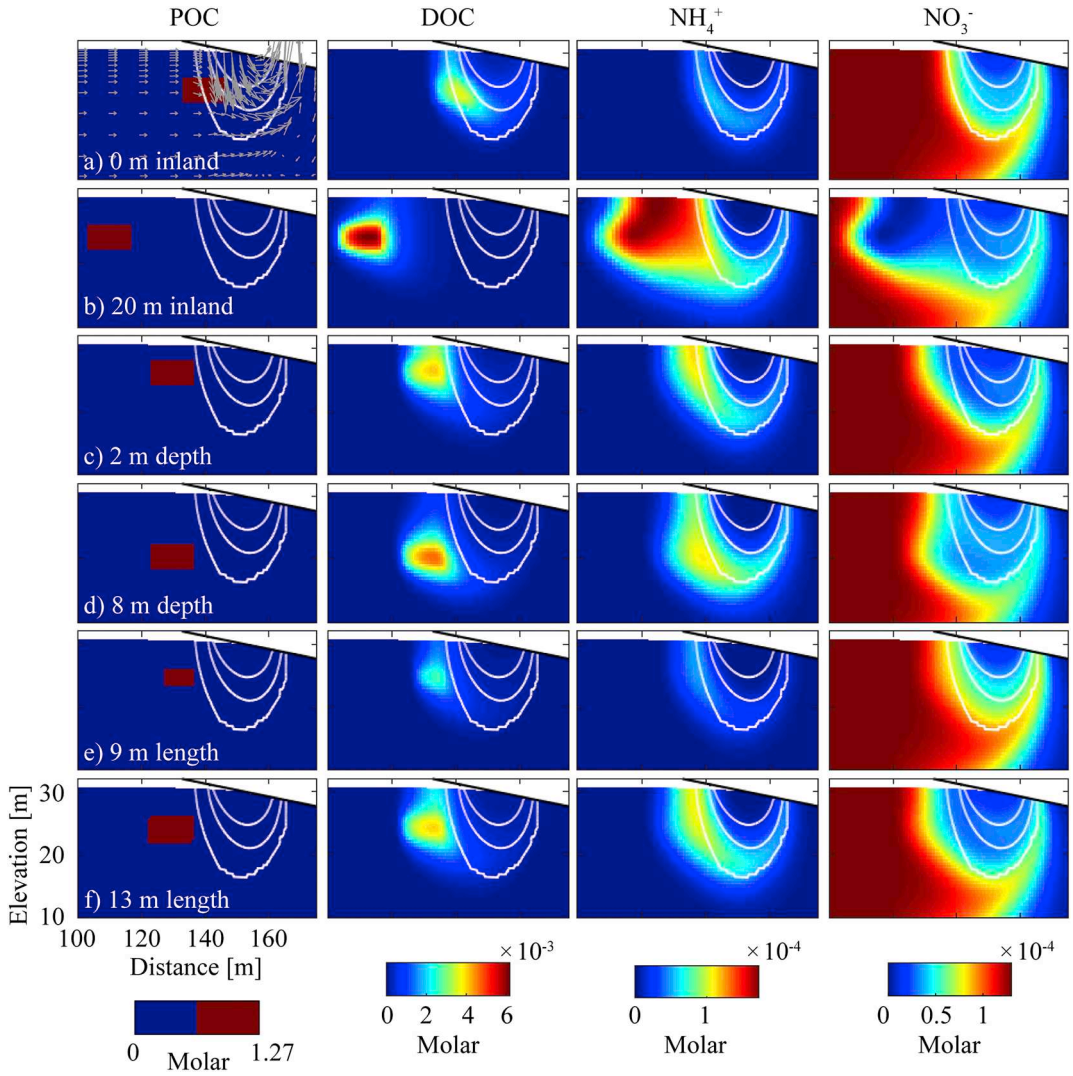

Fig. 3. Modeled concentrations for selected sets of whale burial distances inland from the high tide line (rows a-b), burial depth (rows c-d), and whale length (rows e-f). White contours are 1%, 10% and 90% seawater salinity. Flow vectors for all panels are shown in panel (a).

with increasing burial size (Fig. 6f). DOC degradation is coupled to ammonification and thus NH_4^+ flux across the aquifer-ocean interface increased with setback distance and depth (Fig. 6g-h). Unlike setback distance and burial depth, where NH_4^+ flux varied inversely with DOC flux, the model results show that both NH_4^+ and DOC flux increased with whale size. The four burials of different sizes were set in an identical location in the flow system. This eliminated the effects of hydrological variation such as transport rates that contributed to the inverse relationship between DOC and NH_4^+ flux for differences in setback distance and burial depth.

3.5. Buried wrack: solute concentrations and denitrification zone

Buried wrack aggregates altered the distribution of solutes in the beach aquifer. Fig. 7 shows solute concentrations in sediments with 10–100% POC content. Decomposition of the wrack generated DOC that accumulated along circulating flow paths (Fig. 7, row 2). DOC fueled aerobic respiration in the shallow beach subsurface, however O_2 concentrations remained elevated enough to inhibit denitrification in pore water greater than 50% seawater in the circulation cell (Figs. 7 and 8). On the boundary of the circulation cell in pore water with salinity less than 50% seawater, land-derived NO_3^- mixed with DOC in anoxic pore water and denitrified as it was transported seaward (Fig. 8). An increase in buried wrack content and corresponding increase in DOC led to enhanced NO_3^- removal and lower NO_3^- concentrations in the fresh discharge zone (Fig. 7, row 4).

The baseline model and the wrack aggregate models both show that denitrification occurred in the intertidal mixing zone in pore water with salinity less than 50% seawater, however reaction rates were highest on opposite ends of the circulation cell; the landward side when seawater was the source of DOC and on the seaward side when wrack aggregates were the source of DOC (Fig. 2f and Fig. 8). Denitrification rates for the baseline model were highest on the landward side of the circulation cell because infiltrating seawater transported large quantities of DOC into the aquifer below the high tide line, while the accumulation of DOC in the wrack simulations led to high NO_3^- removal rates at the terminal end of circulating flow paths.

4. Sensitivity analysis: effects of model parameters

4.1. Whale burial leachate fluxes

DOC and ammonium fluxes to surface water varied with beach properties, hydrologic forcing, and reaction parameter values. Fig. 9 shows the percent change in DOC and ammonium flux relative to the base case parameter set and base case burial scenario for a range of physical and reaction parameter values. Hydraulic conductivity was the most important physical parameter affecting leachate fluxes, followed

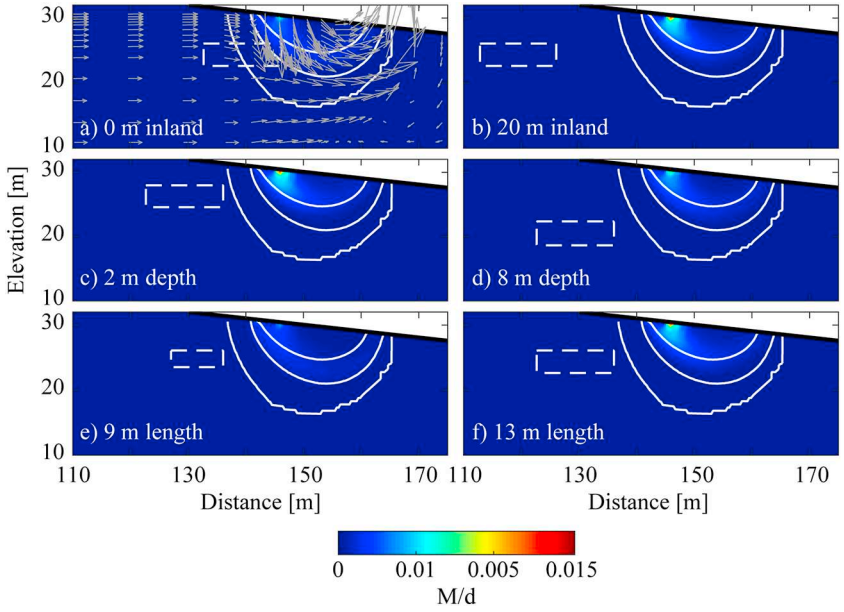

Fig. 4. Nitrification rates for selected sets of whale burial distances inland from the high tide line (a-b), burial depth (c-d), and whale length (e-f). Solid white contours are 1%, 10% and 90% seawater salinity and the dotted white contour signifies the whale burial. Flow vectors for all panels are shown in panel (a).

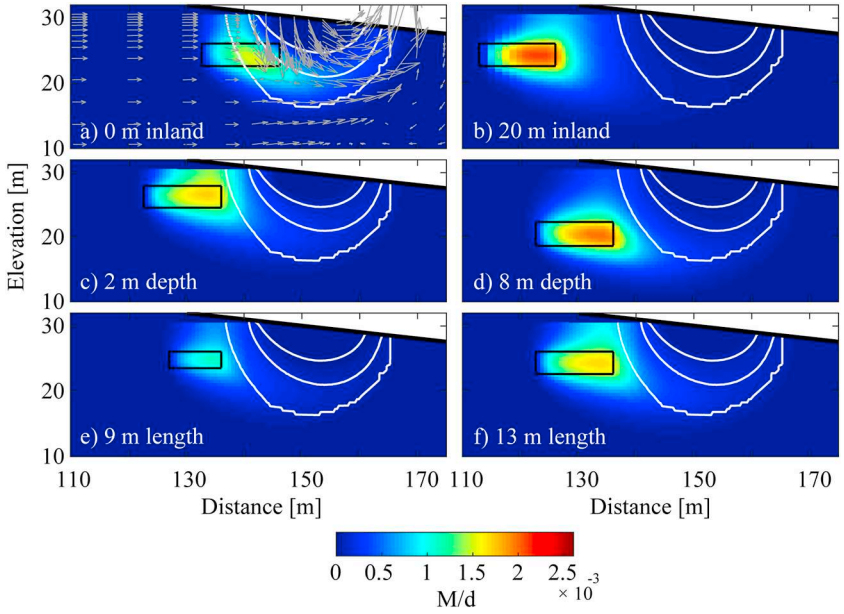

Fig. 5. Denitrification rates for selected sets of whale burial distances inland from the high tide line (a-b), burial depth (c-d), and whale length (e-f). White contours are 1%, 10% and 90% seawater salinity and the black contour signifies the whale burial location.

by the tidal amplitude, anisotropy ratio, beach slope, freshwater hydraulic gradient, transverse dispersivity ratio, and longitudinal dispersivity. DOC flux increased with hydraulic conductivity due to higher transport rates between the whale burial and discharge zone, limiting DOC degradation and ammonification (Fig. 9a). DOC and ammonium leachate fluxes varied between −69.5% and 176.6% relative to the base case for hydraulic conductivity values of 2–50 m/d. Tidal amplitude was the second most important physical factor, with DOC and ammonium fluxes varying between −72.1% and 128.5% around the base case for tidal amplitudes between 0.2 m and 1.3 m. DOC flux decreased with increasing tidal amplitude due to longer circulating intertidal flow paths that led to greater DOC degradation, but it was met with a corresponding increase in ammonium flux (Fig. 9b). Beach slope had a moderate impact on DOC and ammonium fluxes. Fluxes varied from −67.5% - 70.2% for beach slopes between 0.0375 and 0.1. Steeper beaches formed smaller circulation cells owing to narrower intertidal zones, which shortened transport paths between the whale burial and discharge zone. Thus, DOC fluxes increased with beach slope due to less DOC degradation, while ammonium fluxes decreased as a result of diminished ammonification (Fig. 9c). The freshwater hydraulic gradient was also an important factor affecting leachate flux (Fig. 9d). Strong freshwater hydraulic gradients restricted tidally-driven flows, which resulted in shorter flow paths between the whale burial and discharge zone. Combined with shorter freshwater residence times, this led to higher DOC fluxes, while simultaneously limiting ammonification (Fig. 9d). DOC and ammonium fluxes varied between −62.5% and 40.5% relative to the base case across the range of freshwater hydraulic gradients. The transverse dispersivity ratio and longitudinal dispersivity had a negligible effect on DOC and ammonium fluxes because DOC degradation and ammonification occurred as mixing-independent

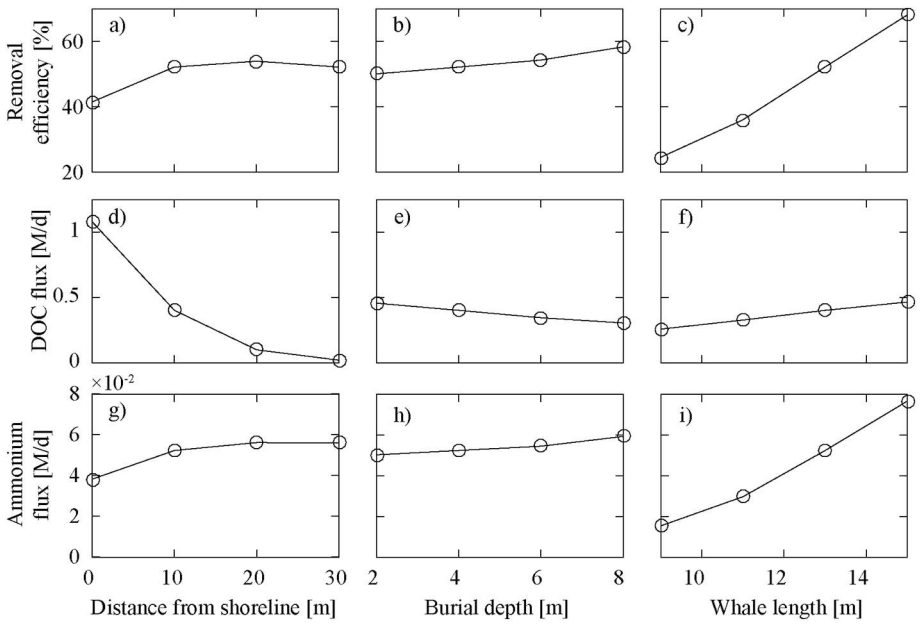

Fig. 6. Whale leachate model results showing the effects of burial distance inland from the shoreline, burial depth, and whale length on percent of nitrate removed and total DOC and ammonium (NH_4^+) flux to coastal surface water per meter length of shoreline.

reactions (Fig. 9e-f). These results highlight the importance of physical hydrologic controls on the fate of whale leachate in beach aquifers.

Leachate fluxes were also sensitive to reaction model parameters. The mass transfer coefficient for organic carbon was the most important reactive parameter affecting DOC and ammonium flux to the subtidal zone, with fluxes varying between −77.7% and 110.2% relative to the base case for the range of tested mass transfer coefficients (Fig. 9h). Increases in both the mass transfer coefficient and distribution coefficient enhanced dissolution of POC and resulted in higher DOC and ammonium fluxes (Fig. 9h-i). As expected, higher DOC rate constants led to lower DOC fluxes as more DOC was consumed along flow paths, while ammonium fluxes increased owing to more rapid ammonification (Fig. 9j).

4.1.1. Buried wrack nitrate removal

The results of the parametric sensitivity analysis provide an upper and lower bound of leachate fluxes and nitrate removal efficiencies for the best estimate parameter values used in the base case burial scenario. For the base case parameter set and burial scenario, nitrate removal efficiency increased from 1.6–30.3% as intertidal POC content increased from 10 to 100% (black symbology; Fig. 10), while the removal efficiency was 37.4% for the baseline model with seawater as the source of DOC (not shown). However, the model sensitivity analysis showed that removal efficiency depends on physical beach properties and reaction parameter values. Removal efficiency was most sensitive to beach slope, varying by an average of 55.8% (range = 0–55.8% relative to base case) across all POC contents for slopes from 0.1 to 0.0375 (Fig. 10c). Wider intertidal zones supported larger circulation cells with more wrack deposition, leading to greater DOC production and larger denitrification zones. The freshwater hydraulic gradient and hydraulic conductivity had a similar effect on removal efficiency. Removal efficiency across the range of freshwater hydraulic gradients (0.0083–0.003) and hydraulic conductivity values (2–50 m/d) varied, respectively, by an average of 29.0% (range = −8.6-20.4% relative to base case) and 28.7% (range = −4.0-24.7% relative to base case) across all POC contents (Fig. 10a and d). Tidal amplitude had a moderate influence on removal efficiency, differing by 19.7% (range = −11.3-8.4% relative to base case) for amplitudes between 0.2 m and 1.3 m. The effects of anisotropy were less, with a mean variability of 8.8% (range = 0–8.8% relative to base case) for anisotropy ratios of 0.1–1.0 (Fig. 10g). The combination of factors that resulted in large intertidal mixing zones (i.e. gentle beach slope, low freshwater hydraulic gradient, high K, large tidal amplitude) yielded higher removal efficiencies due to larger accumulations of wrack and associated DOC production, as well as greater contact between nitrate-rich fresh groundwater and anoxic circulating seawater. For a detailed description of the role of each physical factor on physical flow and transport in beach aquifers, see Heiss et al. (2017). Removal efficiency varied by 6.2% (range = −2.6-3.6% relative to base case) for transverse dispersivity ratios between 0.01 and 0.2, and by 2.3% (range = −0.9-1.4% relative to base case) for longitudinal dispersivity values ranging from 0.1–1.0 m (Fig. 10e and f).

The distribution coefficient was a key reaction parameter affecting removal efficiency (56.3% variability relative to base case), followed by the mass transfer coefficient (29.5%) and DOC rate constant (25.2%). As discussed in Section 3.5.1, larger distribution and mass transfer coefficients enhanced DOC production. The greater DOC availability, which was also supported by lower DOC rate constants, promoted denitrification and increased removal efficiency for the range of parameter values tested.

5. Discussion

5.1. Whale burial implications for shark attraction

The discharging concentration of DOC and NH_4^+ relative to the surface water concentration is likely a primary factor determining the formation of surface water leachate plumes that could potentially serve as a shark attractant. Simulation results based on the base case set of parameters show that maximum DOC concentrations in discharging leachate near the low tide line can reach 660 μM, while observed ambient DOC concentrations in coastal waters worldwide ranges from 180 to 420 μM (Bauer and Bianchi, 2012). Thus, leached DOC concentrations in submarine groundwater discharge may be up to 1.6 times higher than in coastal surface water. Similarly, the maximum NH_4^+ concentration of discharging leachate for models using the base case parameter set was 56 μM, more than an order of magnitude higher than 2 μM typical of surf zones (Pregnall and Miller, 1988). These findings may have implications for shark attraction to areas where whale leachate is discharging to surface water.

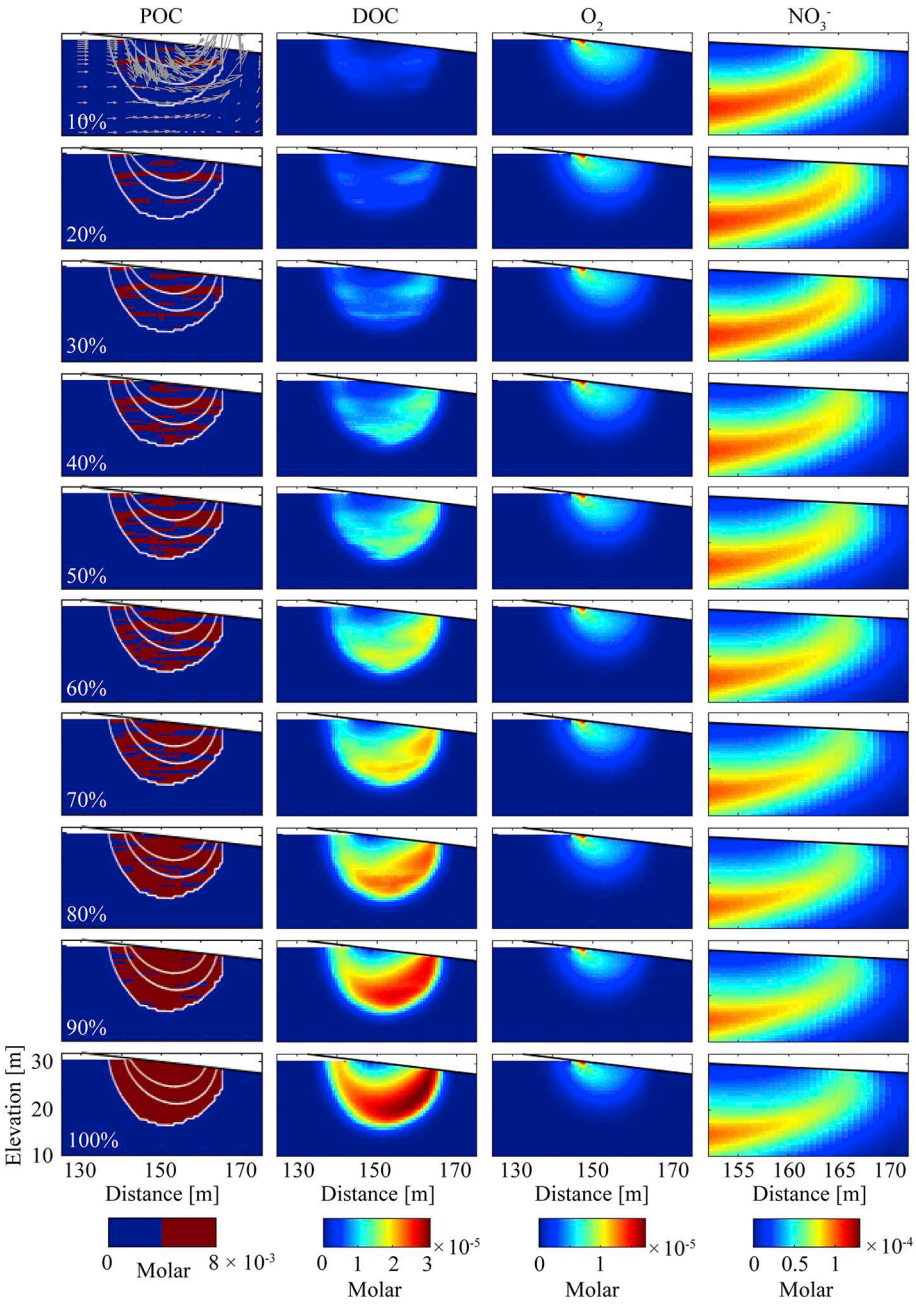

Fig. 7. Model results showing POC, DOC, O_2, and NO_3^- concentrations in the beach aquifer for 10–100% POC content for the base case parameter set. White contours are 1%, 10% and 90% seawater salinity.

The depth of the water column where whale leachate discharges may be important for plume dispersal in the subtidal zone. Fig. 11 shows the cross-shore location of the DOC and NH_4^+ discharge zones and the water column depth across the subtidal zone during low, mid, and high tide. The leached DOC discharge zone spans approximately 11 m across the aquifer-ocean interface and is centered 2.0 m seaward of the low tide line, corresponding to a surface water depth of 2.2 m during high tide and 0.9 m during low tide. NH_4^+ fluxes peak 4.1 m seaward of the low tide line where the water depth is 2.4 m at high tide and 0.4 m at low tide. The depth of the water column at the DOC and NH_4^+ discharge zones is typical of water depths occupied by swimmers. Combined with elevated leachate concentrations as discussed above, these results may have important implications for shark attraction to the inner subtidal zone.

For a given leachate concentration and flux to the subtidal zone, surface water DOC and NH_4^+ enrichment will ultimately depend on numerous factors that impact surf and subtidal zone plume dispersal that were not considered in this study, including wave energy, bathymetry, tidal regime, shape of the coastline, water column depth, and biological activity in the surface water. Additionally, the specific compounds in a leachate plume that sharks may be attracted to is unclear, and the stage of DOC degradation and the chemical signature of a leachate plume will evolve along discharging transport pathways with greater complexity than modeled here. The DOC and NH_4^+ fluxes in this study should therefore be considered a first-order estimate of the impact of whale burial decomposition on material fluxes to coastal surface waters.

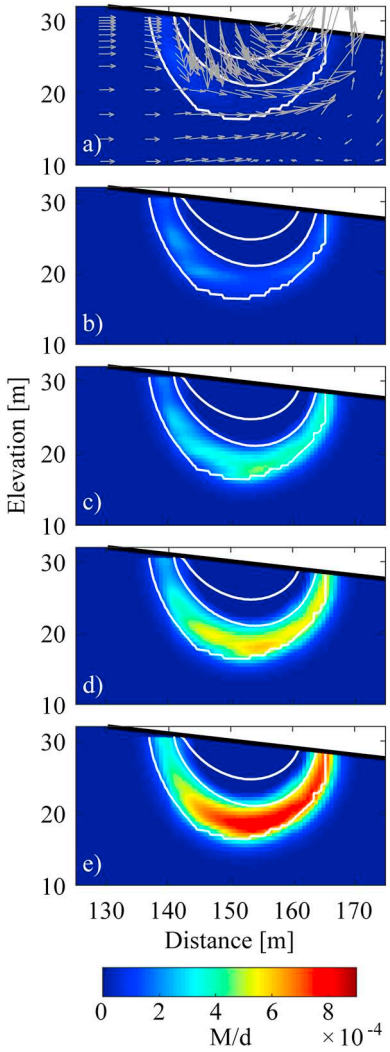

Fig. 8. Denitrification rates (color bar) and salinity (1%, 50%, and 90% seawater salinity; white contours) for an intertidal POC content of a) 10%, b) 30%, c) 50%, d) 70%, and e) 90%.

5.2. Whale burial nitrate attenuation implications

The results of this study provide a framework for predicting the location and magnitude of biogeochemical reactivity in beach aquifers for typical whale burial management decisions. With the rise in global whale populations since the commercial whaling moratorium in 1986 (Tulloch et al., 2018), coastal managers must increasingly weigh the potential risks and benefits of whale disposal methods. The base case model scenario used in this study reveals that whale burials may attenuate up to 68% of land-derived NO_3^- that would otherwise discharge to the coastal ocean ecosystem along the section of the beach where the whale is located. NO_3^- attenuation by whale burials as shown in this study is similar to and is of the same spatial scale as permeable reactive barriers designed to mitigate coastal eutrophication through the supply of carbon from the decomposition of buried woodchips. Hiller et al. (2015) showed that a 20 m long x 3 m diameter woodchip permeable reactive barrier installed in a beach promoted denitrification and led to a decline in nitrate concentrations in discharging groundwater. These artificial nitrogen treatment systems are most effective when installed at the mouth of watersheds where groundwater flow converges at the coast (Barbarso et al., 2019). Thus, although the burials are small (up to 15 m in length in this study) relative to the length of coastline, the burials may have the potential to significantly reduce nitrogen loads to receiving surface water bodies. This newly identified artificial ecosystem service should be considered in decision tools used to assist beach managers, coastal stakeholders, and regulators when evaluating the optimal carcass disposal method for a particular stranding and surface water quality conditions.

The elevated NO_3^- concentrations in inflowing fresh groundwater is representative of densely-populated coastal communities or in areas with continued agricultural development, where increased groundwater loading of N from wastewater and fertilizer to coastal surface water can have adverse ecosystem impacts (Slomp and Van Cappellen, 2004; Valiela et al., 1990). The NO_3^- attenuation capacity of whale burials as shown in this study is therefore most applicable to highly urbanized or rural coastal landscapes.

5.3. Optimal whale burial location

The optimal burial depth and distance inland from the high tide line depends on management goals. The findings suggest that managers should strive for a setback distance >10 m at the maximum achievable depth if coastal waters are susceptible to eutrophication. This burial configuration increases NO_3^- removal efficiency by increasing the residence time of reactive solutes.

If there is concern of shark attraction resulting from burial decomposition and related chemical fluxes, two burial configurations may be considered to limit leachate flux to the subtidal zone. Carcasses buried at high setback distances (>30 m) should result in near-zero DOC flux due to greater DOC degradation along longer flow paths. However, high setback distances result in higher NH_4^+ fluxes, thus an alternate configuration is more suitable to limit NH_4^+ loading. Burials placed below the high tide line (0 m setback distance) at the shallowest burial depth (2 m) should lead to lower NH_4^+ fluxes to surface water, since short transport paths to the discharge zone coupled with rapid circulating flows in the circulation cell decrease the time available for ammonification.

The sensitivity analysis demonstrates that managers should also consider the physical characteristics of the beach and the hydrologic conditions of the coastal aquifer when formulating carcass disposal strategies and selecting burial sites. Model results show that leachate fluxes are highly dependent on beach properties and the hydrologic forces acting on the aquifer. A set of beach (e.g. gentle beach slope, low hydraulic conductivity) and hydrologic (e.g. large tidal amplitude, low freshwater gradient) parameters that increase residence time in the coastal aquifer will reduce DOC delivery to receiving coastal waters owing to greater DOC degradation along flow paths, however the longer residence times will enhance ammonification, yielding higher ammonium fluxes. Prioritization of efforts focused on moderating DOC or ammonium flux from whale burials will depend likely on management goals and ultimately the extent of shark attraction to the leachate compounds considered in this study.

5.4. Beach wrack

The numerical simulations suggest that buried wrack can serve as source of DOC that sustains bulk denitrification at rates that approach those supported by the supply of DOC in infiltrating seawater. These results support field observations of the role of buried wrack on moderating nutrient fluxes to coastal ecosystems (Rossi and Underwood, 2002). In addition, denitrification rates were spatially discontinuous and highest farther along circulating flow paths where DOC accumulated, consistent with observed denitrification patterns that result from scattered pools of carbon within beach sediments (Kim et al., 2019). This has important implications for beach managers engaged in beach grooming, which invokes large machinery to scrape and sieve the sand surface to remove plastics, paper, fishing lines, hooks, and other debris that accumulate on popular beaches. Grooming is also conduced to remove beach wrack and is therefore likely to reduce wrack burial and

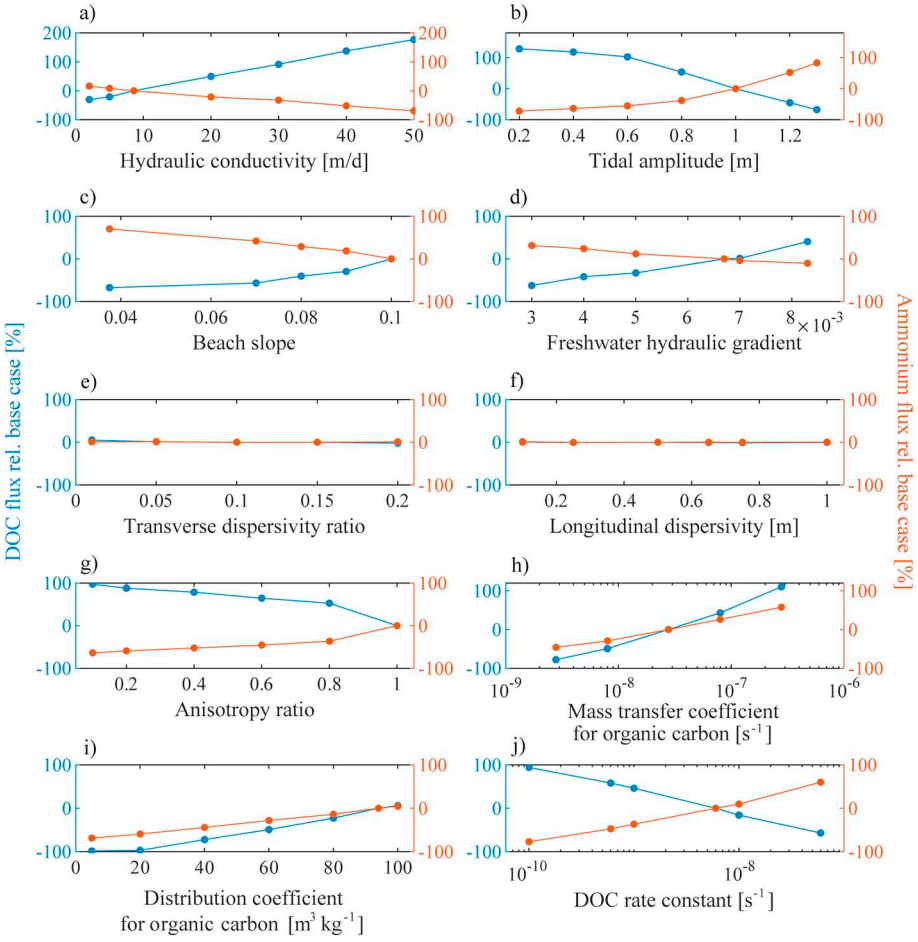

Fig. 9. Sensitivity of DOC and ammonium flux relative to the whale burial base case parameter set and burial scenario (10 m setback distance, 4 m burial depth, and 13 m length) for physical and reaction parameters.

subsequent supply of organic carbon to the beach aquifer, leading to lower NO_3^- attenuation. Coastal armoring is also likely to reduce the quantity of buried wrack and the availability of DOC, as the footprint of armored beach structures covers areas of the beachface where wrack accumulates (Dugan et al. 2008).

5.5. Model simplifications

There are additional factors not accounted for in the models. The models assume that burials are submerged below the water table throughout the tidal cycle. While this may not always be the case, it is a reasonable assumption near the shoreline where vertical infiltration of seawater by wave and tidal action across the beachface maintains shallow water table elevations (e.g. De Dréziguć et al., 2009; Turner et al., 1997) that are above the shallowest burial depth (2 m) identified in media reports in this study. However, shallow burials at high setback distances in high relief areas may be permanently located in the unsaturated zone or periodically inundated by an oscillating water table. Previous work has shown that transport of leachate from whale carcasses buried in the unsaturated zone is minimal (Tucker et al., 2019). Additionally, decomposition of lipids in human graves in unsaturated soils is slowed or halted due limited oxygen availability and exposure to reducing conditions (Dent et al., 2004), further suggesting that whale burials located above the water table are unlikely to produce leachate of sufficient quantity to be transported to surface water. The results of the present study demonstrate that burials below the water table can produce leachate that is transported to the nearshore area by groundwater flow.

Wave setup and swash, spring-neap variability in tidal amplitude, seasonal oscillations in the freshwater hydraulic gradient, and precipitation events affect flow, transport, and mixing in beach aquifers (Abarca et al., 2013; Heiss and Michael, 2014; Heiss et al., 2014; Heiss et al., 2015; Robinson et al., 2007a, 2007b; Robinson et al., 2014; Xin et al., 2010). Oscillatory flows and shifting redox gradients that result from these transient hydrologic forcing mechanisms will may lead to temporal variability in the spatial distribution of reaction zones, reactivity intensity, and chemical fluxes. The dynamic physical flow and chemical responses to these transient and interacting forcings may lead to optimal burial configurations that differ from those found in this study.

The numerical model accounted for N mineralization, nitrification, and denitrification, however additional N cycling pathways have been observed in beach aquifers, such as anaerobic ammonium oxidation (Anammox; Slomp and Van Cappellen, 2004) and dissimilatory nitrate reduction to ammonium (DNRA Santoro, 2010). Annamox would provide an additional N removal pathway that would reduce denitrification though the consumption of NO_3^-. Similarly, DNRA competes with denitrification to reduce NO_3^- and requires the same redox conditions. Thus, actual NO_3^- removal, whether performed via anammox, DNRA, or denitrification, would unlikely deviate significantly from the simulated results if anammox and DNRA were incorporated into the reaction network. NH_4^+ flux to the surface water would likely decrease with the incorporation of anammox owing to NH_4^+ oxidation. Lastly, the modeling approach does not consider interactions between overlapping decomposition plumes in settings with both a whale burial and buried wrack. Both sources of carbon were intentionally not implemented in

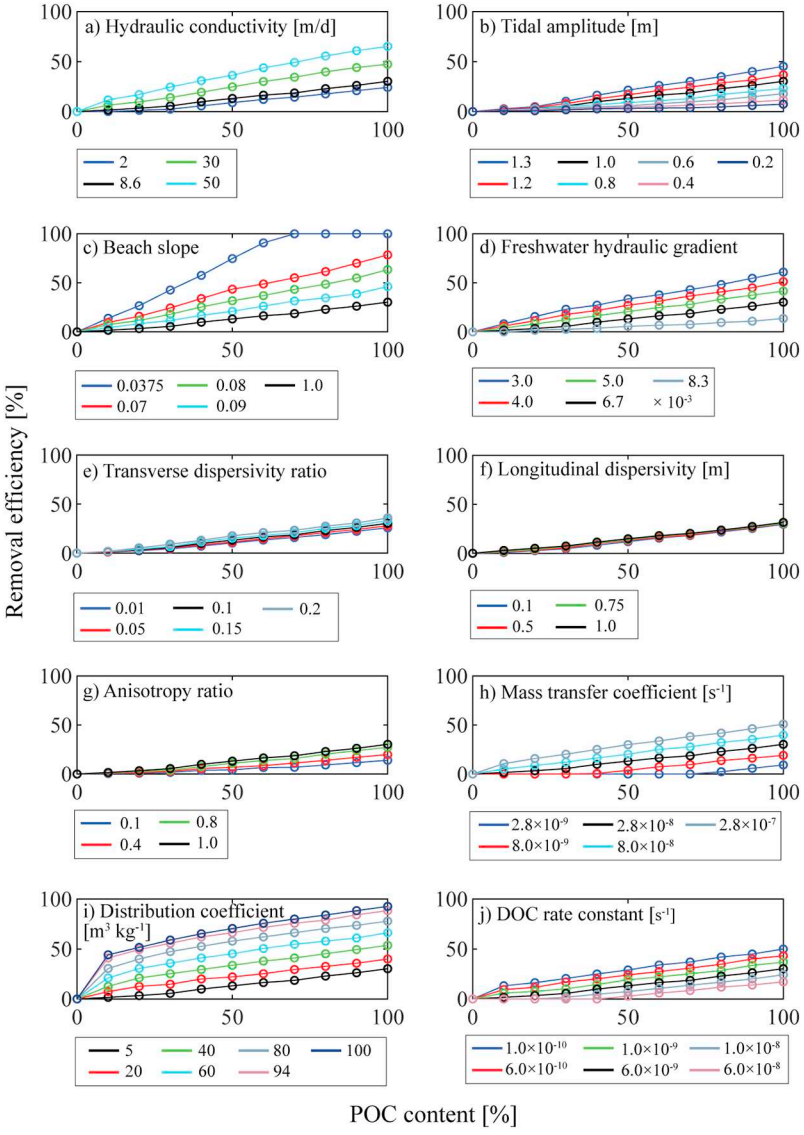

Fig. 10. Nitrate removal sensitivity to physical and reaction parameters for intertidal POC content ranging from 0 to 100%. The base case parameter set is represented by black symbology in all panels.

model scenarios because data on organic carbon content of beach sediments at a potential whale burial site is often unavailable to coastal managers. Thus, the goal was to understand the individual effects of each carbon source to independently support whale disposal and beach scraping management decisions.

6. Conclusions

A reactive transport model was combined with a variable-density groundwater flow model to simulate the effects of whale burial decomposition and buried organic matter (i.e. wrack) on the chemical composition and reactivity of coastal aquifers subjected to tides. The findings demonstrate the importance of whale burial location on whale leachate extent and associated flux to surface water, and the effects of buried wrack on nutrient fluxes to coastal ecosystems. A sensitivity analysis of whale burial distance inland from the high tide line, burial depth, and whale size show that decomposition of whale burials produces DOC and ammonium leachate plumes that are transported to and discharge from the aquifer near the low tide line in water depths between 0.4 and 2.4 m. DOC and ammonium concentrations in discharging leachate for the base case models are 1.6 and 26 times higher than typical surf zone concentrations, respectively.

In instances where there is concern of shark attraction to discharging leachate, two burial configurations may be considered to limit leachate flux to the subtidal zone. Burials located 30 m inland from the high tide line at a depth of 8 m will likely result in near-zero DOC flux. However, this burial configuration enhances ammonium fluxes, thus an alternate configuration is more suitable to limit ammonium loading. Burials placed at shallow depth (2 m) below the high tide line should lead to lower ammonium fluxes to surface water. It should be noted that the model employed in this study assumes that the whales are submerged below the water table, which may not always be the case. Leachate production from whales buried in the unsaturated zone is likely to differ than modeled in the present study.

Simulation results suggest that managers should strive for a setback distance of greater than 10 m at the maximum achievable depth if a management objective is to promote denitrification and reduce N loading to coastal ecosystems. Whale burials serve as a source of DOC that fuels denitrification hotspots surrounding and down-gradient of the burials. Denitrification within the hotspots can remove 41–68% of land-derived NO_3^- prior to discharge along the length of beach where the whale is located for the burial scenarios considered. Whale burials are

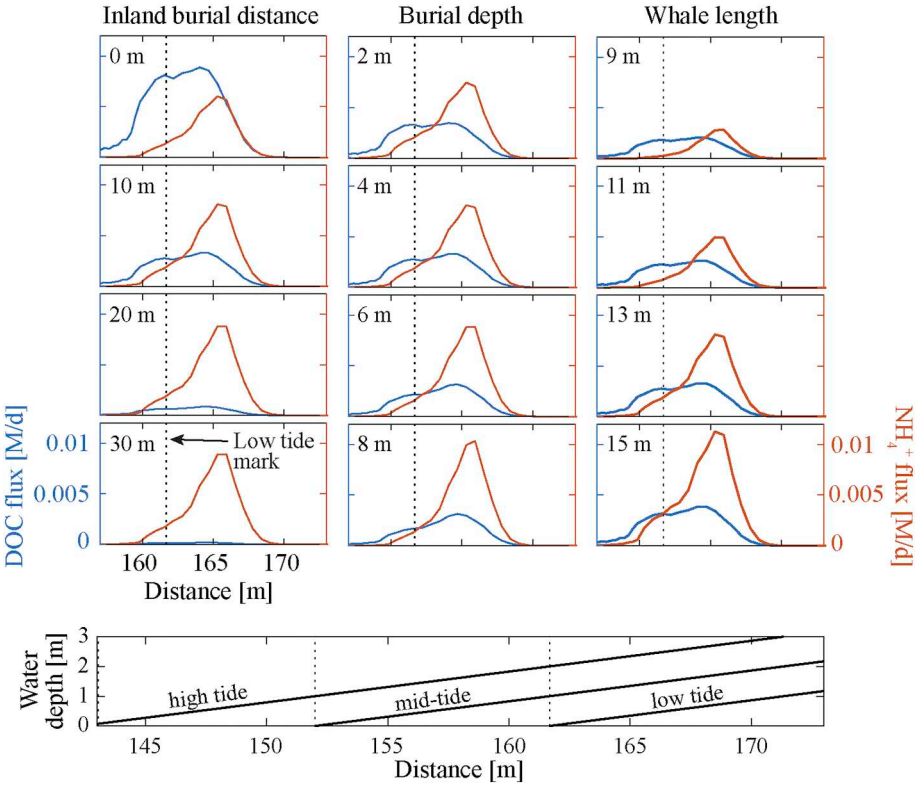

Fig. 11. Whale leachate DOC and ammonium (NH_4^+) fluxes across the aquifer-ocean interface. The bottom panel shows surface water depths during high, mid, and low tide for all burial scenarios based on the base case parameter set.

similar in size to artificial permeable reactive barriers that are installed in coastal aquifers to moderate nitrogen fluxes to coastal ecosystems. These findings demonstrate a potentially new management strategy that may be implemented to help meet nutrient loading goals.

Simulations were performed to evaluate NO_3^- removal efficiencies for a range of buried wrack scenarios. NO_3^- removal increased with increasing sediment organic carbon content and ranged from 1.6 and 30.3% for 10–100% intertidal sediment organic carbon content, while 37.4% of NO_3^- was attenuated with infiltrating seawater as the only source of DOC. Thus, buried wrack is likely to serve as a large source of DOC that fuels N transformations in beach aquifers.

A model sensitivity analysis was performed around the whale burial and wrack base case models for a range of physical beach characteristics, hydrologic forcing conditions, and reaction parameters to provide an upper and lower bound of leachate fluxes and nitrate removal efficiencies. Results indicate that DOC and ammonium fluxes to surface water from whale decomposition can range from −72.1% to 176.6% relative to the base case scenario. Nitrate removal efficiencies can range from 0 to 44.2% for beaches composed of 10% wrack to 7.4–100% for beaches composed of 100% wrack, depending on reaction parameters, beach properties, and hydrologic forcing.

The whale burial model results may have implications for shark attraction to the shallow subtidal zone. Water depth in the whale leachate discharge zone is within the range of swimming depths of beachgoers, and discharging leachate concentrations are higher relative to typical ambient surface water concentrations. The results of this study are based on numerical models with a simplified accounting of N speciation and transformation, and the implications of whale leachate fluxes on shark attraction remains unclear due to limited shark sensory research. It is suggested that future research identify the leachate compounds that are shark attractants and classify the corresponding concentrations that influence shark behavior.

Acknowledgements

I thank Christopher Russoniello and Holly Michael for helpful comments on the manuscript. The model outputs from this study are available on HydroShare at http://www.hydroshare.org/resource/6c604c94779a49b4aea67868f4308364. This manuscript benefited from the valuable comments of three anonymous reviewers.

Declaration of Competing Interest

None.

References

Abarca, E., Karam, H., Hemond, H.F., Harvey, C.F., 2013. Transient groundwater dynamics in a coastal aquifer: the effects of tides, the lunar cycle, and the beach profile. Water Resour. Res. 49 (July 2012), 1–16. https://doi.org/10.1002/wrcr.20075.

Amato, D.W., Bishop, J.M., Glenn, C.R., Dulai, H., Smith, C.M., 2016. Impact of submarine groundwater discharge on marine water quality and reef biota of Maui. PLoS One 11 (11), e0165825. https://doi.org/10.1371/journal.pone.0165825.

Anwar, N., Robinson, C., Barry, D.A., 2014. Influence of tides and waves on the fate of nutrients in a nearshore aquifer: numerical simulations. Adv. Water Resour. 73 (2014), 203–213. https://doi.org/10.1016/j.advwatres.2014.08.015.

Barbaro, J.R., Belaval, M., Truslow, D.B., LeBlanc, D.R., Cambareri, T.C., and Michaud, S. C., 2019, Hydrologic site assessment for passive treatment of groundwater nitrogen with permeable reactive barriers, Cape Cod, Massachusetts: U.S. Geological Survey Scientific Investigations Report 2019–5047, 39 p., https://doi.org/10.3133/sir20195047.

Bardini, L., Boano, F., Cardenas, M.B., Revelli, R., Ridolfi, L., 2012. Nutrient cycling in bedform induced hyporheic zones. Geochim. Cosmochim. Acta 84, 47–61. https://doi.org/10.1016/j.gca.2012.01.025.

Bauer, J.E., Bianchi, T.S., 2012. Dissolved organic carbon cycling and transformation. Treatise on estuarine and coastal science (Vol. 5). Elsevier Inc. https://doi.org/10.1016/B978-0-12-374711-2.00502-7.

Berner, R.A., 1981. Authigenic minerals resulting from organic matter decomposition in modern sediments. Fortschr. Mineral. 59, 117–135.

Boufadel, M.C., 2000. A mechanistic study of nonlinear solute transport in a groundwater – surface water system under steady state and transient hydraulic conditions. Water Resour. Res. 36 (9), 2549–2565.

Bui, A., 2009. Beach burial of cetaceans: implications for conservation, and public health

and safety. School of Applied Sciences, Master of(march) 154.
Brun, A., Engesgaard, P., Cardenas, M.B., 2002. Modelling of transport and biogeochemical processes in pollution plumes: Literature review and model and development. J. Hydrol. 256, 211–227. https://doi.org/10.1016/j.gca.2012.01.025.
Cardenas, M.B., Cook, P.L.M., Jiang, H., Traykovski, P., 2008. Constraining denitrification in permeable wave-influenced marine sediment using linked hydrodynamic and biogeochemical modeling. Earth Planet. Sci. Lett. 275 (1–2), 127–137. https://doi.org/10.1016/j.epsl.2008.08.016.
Charette, M.A., Sholkovitz, E.R., 2006. Trace element cycling in a subterranean estuary: part 2. Geochemistry of the pore water. Geochim. Cosmochim. Acta 70 (4), 811–826. https://doi.org/10.1016/j.gca.2005.10.019.
Charbonnier, C., Anschutz, P., Poirier, D., Bujan, S., Lecroart, P., 2017. Aerobic respiration in a high-energy sandy beach. Marine Chemistry 155, 10–21. https://doi.org/10.1016/j.marchem.2013.05.003.
Clua, E., Chauvet, C., Read, T., Werry, J.M., Lee, S.Y., 2013. Behavioural patterns of a Tiger shark (Galeocerdo cuvier) feeding aggregation at a blue whale carcass in Prony Bay, New Caledonia. Mar. Freshw. Behav. Physiol. 46 (1), 1–20. https://doi.org/10.1080/10236244.2013.773127.
Cooper, H.H., 1959. A hypothesis concerning the dynamic balance of fresh water and salt water in a coastal aquifer. J. Geophys. Res. 64 (4), 461–467. https://doi.org/10.1029/JZ064i004p00461.
Couturier, M., Tommi-Morin, G., Sirois, M., Rao, A., Nozais, C., Chaillou, G., 2017. Nitrogen transformations along a shallow subterranean estuary. Biogeosciences. Biogeosciences 14 (13), 3321–3336. https://doi.org/10.5194/bg-14-3321-2017.
Crook, E.D., Potts, D., Rebolledo-Vieyra, M., Hernandez, L., Paytan, A., 2012. Calcifying coral abundance near low-pH springs: implications for future ocean acidification. Coral Reefs 31 (1), 239–245. https://doi.org/10.1007/s00338-011-0839-y.
De Drézigué, O.D., Sous, D., Lambert, A., Gouaud, F., Rey, V., 2009. Watertable response to tidal forcing in the Truc-Vert sandy beach mean low water. J. Coast. Res. 2009 (56), 1761–1765.
Dent, B.B., Forbes, S.L., Stuart, B.H., 2004. Review of human decomposition processes in soil. Environ. Geol. 45 (4), 576–585. https://doi.org/10.1007/s00254-003-0913-z.
Dugan, J.E., Hubbard, D.M., Rodil, I.F., Revell, D.L., Schroeter, S., 2008. Ecological effects of coastal armoring on sandy beaches. Mar. Ecol. 29, 160–170. https://doi.org/10.1111/j.1439-0485.2008.00231.x.
Dugan, J.E., Hubbard, D.M., Page, H.M., Schimel, J.P., 2011. Marine Macrophyte wrack inputs and dissolved nutrients in Beach Sands. Estuar. Coasts 34 (4), 839–850. https://doi.org/10.1007/s12237-011-9375-9.
Fallows, C., Gallagher, A.J., Hammerschlag, N., 2013. White sharks (Carcharodon carcharias) scavenging on whales and its potential role in further shaping the ecology of an apex predator. PLoS One 8 (4), e60797. https://doi.org/10.1371/journal.pone.0060797.
Ford, R.B., Thrush, S.F., Probert, P.K., 1999. Macrobenthic colonisation of disturbances on an intertidal sandflat: the influence of season and buried algae. Mar. Ecol. Prog. Ser. 191, 163–174. https://doi.org/10.3354/meps191163.
Fujita, K., Shoji, J., Sugimoto, R., Nakajima, T., Honda, H., Takeuchi, M., ... Taniguchi, M., 2019. Increase in Fish Production Through Bottom-Up Trophic Linkage in Coastal Waters Induced by Nutrients Supplied via Submarine Groundwater. Front. Environ. Sci. 7 (June), 1–10. https://doi.org/10.3389/fenvs.2019.00082.
Gelhar, L.W., Welty, C., Rehfeldt, K.R., 1992. A critcal review of data on field-scale dispersion in aquifers. Water Resour. Res. 28 (7), 1955–1974.
Geng, X., Boufadel, M.C., Lee, K., Abrams, S., Suidan, M.T., 2015. Biodegradation of subsurface oil in a tidally influenced sand beach: Impact of hydraulics and interaction with pore water chemistry. Water Resour. Res. 51. https://doi.org/10.1002/2014WR016870.
Greskowiak, J., 2014. Tide-induced salt-fingering flow during submarine groundwater discharge. Geophys. Res. Lett. 41, 6413–6419. https://doi.org/10.1002/2014GL061184.
Gu, C., Hornberger, G.M., Mills, A.L., Herman, J.S., Flewelling, S.A., 2007. Nitrate reduction in streambed sediments: Effects of flow and biogeochemical kinetics. Water Resour. Res. 43 (12), 1–10. https://doi.org/10.1029/2007WR006027.
Hazen, A., 1911. Discussions: Dams on sand foundations. Trans. Am. Soc. Civ. Eng. 73, 199.
Heiss, J.W., Michael, H.A., 2014. Saltwater-freshwater mixing dynamics in a sandy beach aquifer over tidal, spring-neap, and seasonal cycles. Water Resour. Res. 50, 6747–6766. https://doi.org/10.1002/2014WR015574.
Heiss, J.W., Ullman, W.J., Michael, H.A., 2014. Swash zone moisture dynamics and unsaturated infiltration in two sandy beach aquifers. Estuar. Coast. Shelf Sci. 143, 20–31. https://doi.org/10.1016/j.ecss.2014.03.015.
Heiss, J.W., Post, V.E.A., Laattoe, T., Russoniello, C.J., Michael, H.A., 2017. Physical controls on biogeochemical processes in intertidal zones of beach aquifers. Water Resour. Res. 53 (11). https://doi.org/10.1002/2017WR021110.
Heiss, James W., Puleo, J.A., Ullman, W.J., Michael, H.A., 2015. Coupled surface-subsurface hydrologic measurements reveal infiltration, recharge, and discharge dynamics across the swash zone of a sandy beach. Water Resour. Res. 51 (11), 8834–8853. https://doi.org/10.1002/2015WR017395.
Hiller, K.A., Foreman, K.H., Weisman, D., Bowen, J.L., 2015. Permeable Reactive Barriers Designed To Mitigate Eutrophication Alter Bacterial Community Composition and Aquifer Redox Conditions. Appl. Environ. Microbiol. 81 (20), 7114–7124. https://doi.org/10.1128/aem.01986-15.
Hill, D.F. (2016). Spatial and Temporal Variability in Tidal Range: Evidence, Causes, and Effects. Current Climate Change Reports. Springer. https://doi.org/10.1007/s40641-016-0044-8.
Huettel, M., Rusch, A., 2000. Advective particle transport into permeable sediments-evidence from experiments in an intertidal sandflat. Limnol. Oceanogr. 45 (3), 525–533. https://doi.org/10.4319/lo.2000.45.3.0525.
Jardine, P.M., Dunnivant, F.M., McCarthy, J.F., Selim, H.M., 1992. Comparison of models for describing the transport of dissolved organic carbon in aquifer columns. Soil Sci. Soc. Am. J. 56 (2), 393. https://doi.org/10.2136/sssaj1992.03615995005600020009x.
Kim, K.H., Heiss, J.W., Michael, H.A., Cai, W.J., Laattoe, T., Post, V.E.A., Ullman, W.J., 2017. Spatial patterns of groundwater biogeochemical reactivity in an Intertidal Beach aquifer. J. Geophys. Res. Biogeosci. 122 (10), 2548–2562. https://doi.org/10.1002/2017JG003943.
Kim, K.H., Michael, H.A., Field, E.K., Ullman, W.J., 2019. Hydrologic shifts create complex transient distributions of particulate organic carbon and biogeochemical responses in beach aquifers. J. Geophys. Res. Biogeosci. 124, 3024–3038. https://doi.org/10.1029/2019JG005114.
Kohout, F.A., 1960. Cyclic flow of salt water in the Biscayne aquifer of southeastern Florida. J. Geophys. Res. 65 (7), 2133–2141. https://doi.org/10.1029/JZ065i007p02133.
Kroeger, K.D., Charette, M.A., 2008. Nitrogen biogeochemistry of submarine groundwater discharge. Limnol. Oceanogr. 53 (3), 1025–1039. https://doi.org/10.4319/lo.2008.53.3.1025.
Langevin, C.D., Thorne Jr., D.T., Dausman, A.M., Sukop, M.C., Guo, W., 2008. SEAWAT version 4: a computer program for simulation of multi-species solute and heat transport, no. 6–A22. Geol. Survey (US). 6 (A22), 39.
Lebbe, L., 1999. Parameter identification in fresh-saltwater flow based on borehole resistivities and freshwater head data. Adv. Water Resour. 22 (8), 791–806.
Lecher, A.L., Mackey, K.R.M., 2018. Synthesizing the effects of submarine groundwater discharge on marine biota. Hydrology, di 1–21. https://doi.org/10.3390/hydrology5040060.
Lecher, A.L., Mackey, K., Kudela, R., Ryan, J., Fisher, A., Murray, J., Paytan, A., 2015. Nutrient loading through submarine groundwater discharge and phytoplankton growth in Monterey bay, CA. Environ. Sci. Technol. 49 (11), 6665–6673. https://doi.org/10.1021/acs.est.5b00909.
Lirman, D., Orlando, B., Maciá, S., Manzello, D., Kaufman, L., Biber, P., Jones, T., 2003. Coral communities of Biscayne Bay, Florida and adjacent offshore areas: diversity, abundance, distribution, and environmental correlates. Aquat. Conserv. Mar. Freshwat. Ecosyst. 13 (2), 121–135. https://doi.org/10.1002/aqc.552.
MacQuarrie, K.T.B., Sudicky, E.A., Robertson, W.D., 2001. Numerical simulation of a fine-grained denitrification layer for removing septic system nitrate from shallow groundwater. J. Contam. Hydrol. 52, 29–55.
McAllister, S., Barnett, J.M., Heiss, J.W., Findlay, A.J., Macdonald, D.J., Dow, C.L., ... Chan, C.S., 2015. Dynamic hydrologic and biogeochemical processes drive microbially enhanced iron and sulfur cycling within the intertidal mixing zone of a beach aquifer. Limnology and Oceanography 60 (1), 329–345. https://doi.org/10.1111/lno.10029.
Michael, H.A., Mulligan, A.E., Harvey, C.F., 2005. Seasonal oscillations in water exchange between aquifers and the coastal ocean. Nature 436 (7054), 1145–1148. https://doi.org/10.1038/nature03935.
Miller, C.A., Best, P.B., Perryman, W.L., Baumgartner, M.F., Moore, M.J., 2012. Body shape changes associated with reproductive status, nutritive condition and growth in right whales Eubalaena glacialis and E. australis. Mar. Ecol. Prog. Ser. 459 (Iwc 2001), 135–156. https://doi.org/10.3354/meps09675.
Orr, M., Zimmer, M., Jelinski, D.E., Mews, M., 2005. Wrack deposition on different beach types: spatial and temporal variation in the pattern of subsidy. Ecology 86 (6), 1496–1507.
Paerl, H.W., 1997. Coastal eutrophication and harmful algal blooms: importance of atmospheric deposition and groundwater as new nitrogen and other nutrient sources. Limnol. Oceanogr. 42 (5_part_2), 1154–1165. https://doi.org/10.4319/lo.1997.42.5_part_2.1154.
Post, V.E.A., 2011. Computers & geosciences a new package for simulating periodic boundary conditions in MODFLOW and SEAWAT. Comput. Geosci. 37 (11), 1843–1849. https://doi.org/10.1016/j.cageo.2011.01.012.
Postma, D., Jakobsen, R., Cardenas, M.B., 1996. Redox zonation: equilibrium constraints on the Fe (III)/SO4-reduction interface. Geochim. Cosmochim. Acta 60, 3169–3175 (42).
Prado, J.H.F., Mattos, P.H., Silva, K.G., Secchi, E.R., 2016. Long-Term Seasonal and Interannual Patterns of Marine Mammal Strandings in Subtropical Western South Atlantic. pp. 1–23. https://doi.org/10.1371/journal.pone.0146339.
Pregnall, A., Miller, S., 1988. Flux of ammonium from surf-zone and nearshore sediments in Nahant Bay, Massachusetts, USA, in relation to free-living Pilayella littoralis. Mar. Ecol. Prog. Ser. 50, 161–167. https://doi.org/10.3354/meps050161.
Quanrud, D.M., Arnold, R.G., Wilson, L.G., Gordon, H.J., Graham, D.W., Amy, G.L., 1996. Fate of organics during column studies of soil aquifer treatment. J. Environ. Eng. 122 (4), 314–321.
Robertson, W.D., Cherry, J.A., 1995. In Situ Denitrification of Septic-System Nitrate Using Reactive Porous Media Barriers: Field Trials. Ground Water 33 (1), 99–111. https://doi.org/10.1111/j.1745-6584.1995.tb00266.x.
Robinson, C., Gibbes, B., Li, L., 2006. Driving mechanisms for groundwater flow and salt transport in a subterranean estuary. Geophys. Res. Lett. 33 (3), L03402. https://doi.org/10.1029/2005GL025247.
Robinson, C., Gibbes, B., Carey, H., Li, L., 2007a. Salt-freshwater dynamics in a subterranean estuary over a spring-neap tidal cycle. J. Geophys. Res. 112 (C9), 1–15. https://doi.org/10.1029/2006JC003888.
Robinson, C., Li, L., Barry, D.A., 2007b. Effect of tidal forcing on a subterranean estuary. Adv. Water Resour. 30 (4), 851–865. https://doi.org/10.1016/j.advwatres.2006.07.006.
Robinson, C., Li, L., Prommer, H., 2007c. Tide-induced recirculation across the aquifer-ocean interface. Water Resour. Res. 43 (7), 1–14. https://doi.org/10.1029/2006WR005679.

Robinson, C., Brovelli, A., Barry, D.A., Li, L., 2009. Tidal influence on BTEX biodegradation in sandy coastal aquifers. Adv. Water Resour. 32 (1), 16–28. https://doi.org/10.1016/j.advwatres.2008.09.008.

Reis, a.H., Gama, C., 2010. Sand size versus beachface slope — An explanation based on the Constructal Law. Geomorphology 114 (3), 276–283.

Robinson, C., Xin, P., Li, L., Barry, D.A., 2014. Groundwater flow and salt transport in a subterranean estuary driven by intensified wave conditions. Water Resour. Res. 50 (November 2013), 165–181. https://doi.org/10.1002/2013WR013813.

Rossi, F., Underwood, A.J., 2002. Small-scale disturbance and increased nutrients as influences on intertidal macrobenthic assemblages: experimental burial of wrack in different intertidal environments. Mar. Ecol. Prog. Ser. 241, 29–39. https://doi.org/10.3354/meps241029.

Roy, M., Martin, J.B., Cherrier, J., Cable, J.E., Smith, C.G., 2010. Influence of sea level rise on iron diagenesis in an East Florida subterranean estuary. Geochim. Cosmochim. Acta 74 (19), 5560–5573. https://doi.org/10.1016/j.gca.2010.07.007.

Russoniello, C.J., Konikow, L.F., Kroeger, K.D., Fernandez, C., Andres, A.S., Michael, H.A., 2016. Hydrogeologic controls on groundwater discharge and nitrogen loads in a coastal watershed. J. Hydrol. 538, 783–793. https://doi.org/10.1016/j.jhydrol.2016.05.013.

Sakita, S., Kusuda, T., 2000. Modeling and simulation with microsites on vertical concentration profiles in sediments of aquatic zones. Water Sci. Technol. 42 (3–4), 409–415. https://doi.org/10.2166/wst.2000.0411.

Santoro, A.E., 2010. Microbial nitrogen cycling at the saltwater–freshwater interface. Hydrogeol. J. 18 (1), 187–202. https://doi.org/10.1007/s10040-009-0526-z.

Santos, I.R., Burnett, W.C., Chanton, J., Mwashote, B.M., Suryaputra, I.G.N.A, Dittmar, T., 2008. FNutrient biogeochemistry in a Gulf of Mexico subterranean estuary and groundwater-derived fluxes to the coastal ocean. Limnol. Oceanogr. 53 (2), 705–718. https://doi.org/10.4319/lo.2008.53.2.0705.

Santos, I.R., Burnett, W.C., Dittmar, T., Suryaputra, I.G.N.A., Chanton, J., 2009. Tidal pumping drives nutrient and dissolved organic matter dynamics in a Gulf of Mexico subterranean estuary. Geochim. Cosmochim. Acta 73 (5), 1325–1339. https://doi.org/10.1016/j.gca.2008.11.029.

Sawyer, A.H., 2015. Enhanced removal of groundwater-borne nitrate in heterogeneous aquatic sediments. Geophys. Res. Lett. 42 (2), 403–410. https://doi.org/10.1002/2014GL062234.

Seibert, S.L., Greskowiak, J., Prommer, H., Böttcher, M.E., Massmann, G., 2019. Modeling of biogeochemical processes in a barrier island freshwater lens (Spiekeroog, Germany). J. Hydrol. 575 (February), 1133–1144. https://doi.org/10.1016/j.jhydrol.2019.05.094.

Seidel, M., Beck, M., Greskowiak, J., Riedel, T., Waska, H., Suryaputra, I.G.N.A., ... Dittmar, T., 2015. Biogeochemistry of dissolved organic matter in an intertidal sandy beach. Marine Chemistry 176, 150–163. https://doi.org/10.1016/j.marchem.2015.08.011.

Slomp, C.P., Van Cappellen, P., 2004. Nutrient inputs to the coastal ocean through submarine groundwater discharge: controls and potential impact. J. Hydrol. 295 (1–4), 64–86. https://doi.org/10.1016/j.jhydrol.2004.02.018.

Spiteri, C., Slomp, C.P., Charette, M.A., Tuncay, K., Meile, C., 2008a. Flow and nutrient dynamics in a subterranean estuary (Waquoit Bay, MA, USA): Field data and reactive transport modeling. Geochim. Cosmochim. Acta 72 (14), 3398–3412. https://doi.org/10.1016/j.gca.2008.04.027.

Spiteri, C., Slomp, C.P., Tuncay, K., Meile, C., 2008b. Modeling biogeochemical processes in subterranean estuaries: effect of flow dynamics and redox conditions on submarine groundwater discharge of nutrients. Water Resour. Res. 44 (2). https://doi.org/10.1029/2007WR006071.

Todd, D.K., 1980. Ground-Water Hydrology. John Wiley and Sons, New York, pp. 535.

Tucker, J.P., Santos, I.R., Crocetti, S., Butcher, P., 2018. Whale carcass strandings on beaches: management challenges, research needs, and examples from Australia. Ocean Coast. Manag. 163 (January), 323–338. https://doi.org/10.1016/j.ocecoaman.2018.07.006.

Tucker, J.P., Santos, I.R., Davis, K.L., Butcher, P.A., 2019. Whale carcass leachate plumes in beach groundwater: a potential shark attractant to the surf? Mar. Pollut. Bull. 140 (November 2018), 219–226. https://doi.org/10.1016/j.marpolbul.2019.01.043.

Tulloch, V.J.D., Plagányi, É.E., Matear, R., Brown, C.J., Richardson, A.J., 2018. Ecosystem modelling to quantify the impact of historical whaling on southern hemisphere baleen whales. Fish Fish. 19 (1), 117–137. https://doi.org/10.1111/faf.12241.

Turner, I.L., Acworth, R.I., 2004. Field measurements of Beachface salinity structure using cross-borehole resistivity imaging. J. Coast. Res. 20 (3), 753–760.

Turner, I.L., Coates, B.P., Acworth, R.I., Winter, F., Turnert, I.L., 1997. Tides, waves and the super-elevation of groundwater at the coast. J. Coast. Res. 13 (1), 46–60.

Ullman, W.J., Chang, B., Miller, D.C., Madsen, J.A., 2003. Groundwater mixing, nutrient diagenesis, and discharges across a sandy beachface, Cape Henlopen, Delaware (USA). Estuar. Coast. Shelf Sci. 57 (3), 539–552. https://doi.org/10.1016/S0272-7714(02)00398-0.

Valiela, I., Costa, J., Foreman, K., Teal, J.M.J.M., Howes, B., Aubrey, D., 1990. Transport of groundwater-borne nutrients from watersheds and their effects on coastal waters. Biogeochemistry 10 (3), 177–197. https://doi.org/10.1007/BF00003143.

Valiela, Ivan, McClelland, J., Hauxwell, J., Behr, P.J., Hersh, D., Foreman, K., 1997. Macroalgal blooms in shallow estuaries: Controls and ecophysiological and ecosystem consequences. Limnol. Oceanogr. 42 (5part2), 1105–1118. https://doi.org/10.4319/lo.1997.42.5_part_2.1105.

Van Cappellen, P., Wang, Y., 1996. Cycling of iron and manganese in surface sediments: a general theory for the coupled transport and reaction of carbon, oxygen, nitrogen, sulfur, iron, and manganese. Am. J. Sci. https://doi.org/10.2475/ajs.296.3.197.

Vandenbohede, A., Lebbe, L., 2005. Occurrence of salt water above fresh water in dynamic equilibrium in a coastal groundwater flow system near De Panne, Belgium. Hydrogeol. J. 14 (4), 462–472. https://doi.org/10.1007/s10040-005-0446-5.

Xin, P., Robinson, C., Li, L., Barry, D.A., Bakhtyar, R., 2010. Effects of wave forcing on a subterranean estuary. Water Resour. Res. 46 (12). https://doi.org/10.1029/2010WR009632.

Zarnetske, J.P., Haggerty, R., Wondzell, S.M., Bokil, V.a., González-Pinzón, R., 2012. Coupled transport and reaction kinetics control the nitrate source-sink function of hyporheic zones. Water Resour. Res. 48 (11), 1–15. https://doi.org/10.1029/2012WR011894.

Zektser, I.S., Loaiciga, H.A., 1993. Groundwater fluxes in the global hydrologic cycle: past, present and future. J. Hydrol. 144 (1–4), 405–427. https://doi.org/10.1016/0022-1694(93)90182-9.